Chapter 6

Results and Discussion

We have investigated the interaction of low energy electrons ($0-20$ eV) with molecules condensed on the gold substrate by means of ion desorption. The desorption yields are directly compared with the gas phase and cluster DEA experiments. The experimental results can be interpreted by perturbations of the system by the presence of an environment.

We will present the results from electron stimulated desorption (ESD) from condensed 1,2-$C_2F_4Cl_2$ and SF_5CF_3 molecules. The 1,2-$C_2F_4Cl_2$ also known as Freon 114 was obtained from Messer Griesheim GmbH. The SF_5CF_3 was obtained from Argo Ltd., Essex. Both compounds where used as delivered.

The main part concerns the investigations of a chemical reactions activated by the interaction of low energy electrons with molecules at the surface as will be shown by Cl_2 formation from the condensed 1,2-$C_2F_4Cl_2$.

6.1 Electron initiated reactions in 1,2-$C_2F_4Cl_2$ nanofilms

In this section we will present results obtained from electron attachment experiments to condensed $C_2F_4Cl_2$ molecules. We will first summarize recent results from DEA experiments to gas phase $C_2F_4Cl_2$ and to cluster of $C_2F_4Cl_2$ performed by Langer *et al.* [59] and Fenzlaff [60].

The general trend is, that under collision free conditions formation of NIRs at very low electron energies (< 2 eV) may easyly be identified by monitoring either fragment ions (DEA) or (in particular cases) metastable parent anions. At very low energy, the EA cross-sections are usually very high (in the case of halogen compounds) and may exceed the geometric cross-section of the molecule. In the condensed phase however, when using the ESD technique, observation of resonances below 2 eV is suppressed due to desorption restrictions. On the other hand, formation of higher energy resonances in the gas phase (sometimes barely above the detection limit) may be enhanced in the condensed phase. To understand the influence of the environment on DEA processes, a comparison between the results obtained from gas, cluster and condensed phase measurements has to be made.

As will be shown, the interaction of low energy electrons with a molecular film of $C_2F_4Cl_2$ initiates the synthesis of Cl_2 molecules at the surface. Cl_2 formation proceeds via secondary reactions induced by fragments initially generated by DEA to $C_2F_4Cl_2$. Further measurements then concerns the investigation of the energy dependence of Cl_2 formation, identification of possible reaction routes etc.. Electron driven reactions within condensed environment are known to occur for many molecular systems like for example synthesis of the ozone in the dioxygen matrix [33], CO formation within condensed acetone [61], activation of adsorbed cyclopropane and transformation into propene [62–64], bond selective dissociation of alkanethiol based self-assembled monolayers [65], strand breaks in supercoiled DNA [10, 66], O_2 formation from water ice [36, 37] or modification of $H - Si$ surfaces [67]. However, all mentioned reactions were initiated at incident-electron energies above the threshold of the electronic excitation of the molecule.

We will show, that Cl_2 formation is activated even by subexcitation electrons. Moreover, in the above mentioned examples the generated products were produced in minor amounts with respect to the initial molecule. By extended irradiation of a $C_2F_4Cl_2$ film with 1 eV electrons we were able to transform the initial molecule into molecular chlorine plus by-products (possibly perfluorinated polymers) completely. To identify the reaction routes at subexcitation energies, DEA results from gas phase provide important information.

The last part concerns electron interactions with $C_2F_4Cl_2$ molecules at the surface at submonolayer coverages. Here a relatively thick (> 10ML) rare gas solid as a spacer is used to prevent from perturbation in DEA processes induced by the metallic substrate. Because of the low polarizability of the rare gas atoms, efficiency of the ion desorption at lower impact energies is enhanced and correlation to gas phase results may be done. Since the reaction pathways at the surface strongly depend on the molecular environment, varying the $C_2F_4Cl_2$ concentrations on top of the rare gas film may help to gain further information on the mechanism of Cl_2 synthesis.

6.1.1 DEA to $C_2F_4Cl_2$ molecules in the gas phase and in clusters

Under collision free conditions a variety of negative fragments, formed via electron attachment to single $C_2F_4Cl_2$ molecules, have been observed [59]. They were identified as $Cl^-, Cl_2^-, F^-, ClF^-, CClF_2^-$ and $C_2F_4Cl^-$, see Fig. 6.1. The generation of the negative ions occurs by simple bond cleavage, but also more complex rearrangements of the anionic precursor are involved. All of the observed anionic fragments show resonant features below 4 eV. These features most likely originate from the fragmentation of single particle resonance, formed via capturing of an extra electron into an empty MO. It has been suggested that two distinct transitory negative ion states are responsible for the formation of the negative fragments in the energy region $0-4$ eV. The first state located at 0.5 eV leads to the formation of Cl^-, Cl_2^- and $C_2F_4Cl^-$ ions, while the second state near 2 eV contributes to the formation of all ob-

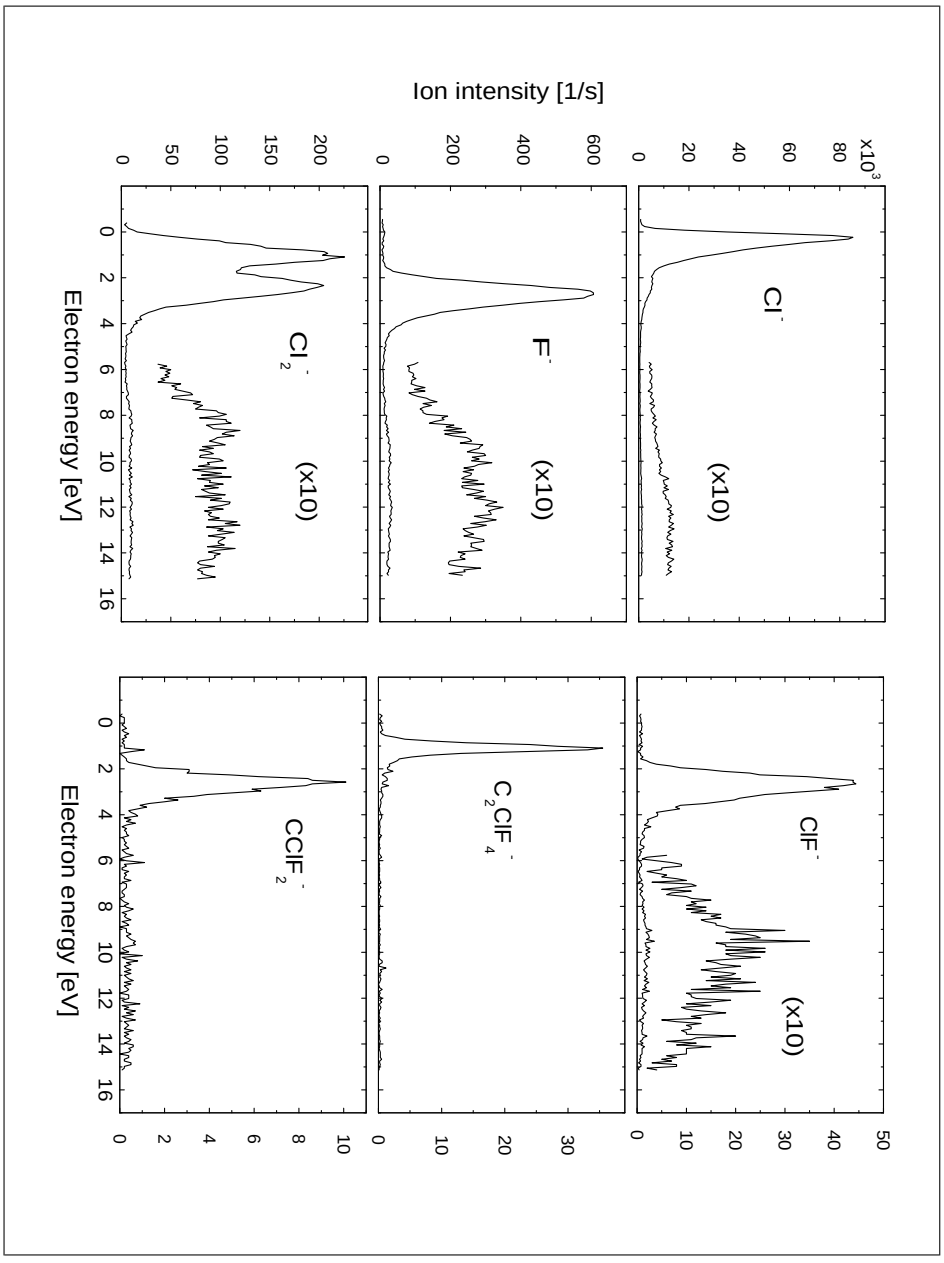

Figure 6.1: *Formation of* Cl^-, F^-, Cl_2^-, ClF^-, $C_2F_4Cl^-$ *and* $CClF_2^-$ *following electron attachment to single* $C_2F_4Cl_2$ *molecules, according to Langer et al. [59].*

served fragments. For the negative ions Cl^-, F^-, Cl_2^- and ClF^- additional resonant like features can be distinguished above 7 eV. At this energy region fragmentation is likely to be initiated by core excited resonances.

The most dominant channel is Cl^-, peaking at 0.3 eV with a small feature around 2.5 eV. The feature between 8 and 14 eV can be associated to the core excited resonances. According to Langer *et al.* [59], the formation of the Cl^- ions below 3 eV has been associated to the reaction

$$e^- + C_2F_4Cl_2 \rightarrow C_2F_4Cl + Cl^- \quad with \quad \Delta H_0 = -0.2 \pm 0.1eV \tag{6.1a}$$

$$e^- + C_2F_4Cl_2 \rightarrow C_2F_4 + Cl + Cl^- \quad with \quad \Delta H_0 = 1.8 \pm 0.1eV \tag{6.1b}$$

The reaction (6.1a) is a simple $Cl - CF_2CF_2Cl$ bond cleavage, while in the reaction (6.1b) multiple fragmentation takes place. The thermodynamical limits were established to be -0.2 ± 0.1 eV for reaction (6.1a) using EA(Cl) = 3.61 eV and $D(Cl - CF_2CClF_2) = 3.4 \pm 0.1$ eV and $= 1.8 \pm 0.1$ eV for the reaction (6.1b) using enthalpies of formation for $C_2F_4Cl_2$ (-937 ± 7 kJmol^{-1}), C_2F_4 (-659 kJmol^{-1}) and Cl (121.3 kJmol^{-1}). From the energetic thresholds it is obvious that reaction (6.1a) is exothermic, while the reaction (6.1b) is endothermic. We can hence conclude that reaction (6.1a) is involved in the Cl^- formation near 0.3 eV, while to Cl^- ion signal at 2.5 eV both dissociation channels (6.1a-6.1b) can contribute.

The F^- ion yield is the second dominant one, however much weaker than the Cl^- signal at 0.3 eV. The F^- ions are formed most likely via a single particle shape resonance. The corresponding reaction is

$$e^- + C_2F_4Cl_2 \rightarrow C_2F_3Cl_2 + F^- \quad with \quad \Delta H_0 = 1.6 \pm 0.1eV \tag{6.2}$$

The thermodynamic threshold was estimated using the electron affinity of F (3.4 eV) and the $F - CFClCF_2Cl$ bond dissociation energy (5.1 eV) [68].

The reaction leading to Cl_2^- formation must obviously include the rearrangement of the intermediate ion since the Cl atoms are bound on the different C atoms and the reaction is unimolecular. The reaction was assigned as

$$e^- + C_2F_4Cl_2 \rightarrow C_2F_4 + Cl_2^- \quad with \quad \Delta H_0 = -0.5 \pm 0.1eV \tag{6.3}$$

here the calculation of ΔH_0 was based on the electron affinity of Cl_2 molecule (2.38 ± 0.1 eV) [68] and the enthalpies of formation for $C_2F_4Cl_2$ and C_2F_4.

The $C_2F_4Cl^-$ dissociative channel is the complement to reaction (6.1a) and is expressed as

$$e^- + C_2F_4Cl_2 \rightarrow C_2F_4Cl^- + Cl \tag{6.4}$$

The observed $C_2F_4Cl^-$ ion yield (its sharp rise of the onset), indicates the opening of the dissociation channel via accessing the threshold limit ΔH_0. Langer *et al.* have derived the electron affinity of $C_2F_4Cl\cdot$ radical to be about 2.9 ± 0.1 eV. However, there is no information about the internal excitation of $C_2F_4Cl^-$ fragment, therefore the obtained value represents the *lower limit* of the electron affinity.

ClF^- and $CClF_2^-$ formation are due to the following reactions

$$e^- + C_2F_4Cl_2 \rightarrow C_2F_3Cl + ClF^- \tag{6.5}$$

$$e^- + C_2F_4Cl_2 \rightarrow CF_2Cl + CF_2Cl^- \tag{6.6}$$

The ClF^- negative ion (6.5) is generated via the cleavage of both $Cl-C$ and $F-C$ bonds either from the same or from different C atoms. The products of the reaction (6.6) are formed via breaking the ClF_2C-CF_2Cl bond. From the recorded ClF^- and CF_2Cl^- ion yields the lower limits of electron affinities have been estimated as EA(ClF) = 1.8 eV $\pm$0.1 eV and EA(CF_2Cl) = 2.1 eV.

Low energy electron impact to $C_2F_4Cl_2$ clusters generates stabilized negative parent ion M^- ($M = C_2F_4Cl_2$). The yield function of M^- follows that of Cl^- ion recorded in the gas phase and cluster measurements. From these observations it has been suggested:

1. The $C_2F_4Cl_2$ molecule possess a positive electron affinity. According to Langer et al. its values was estimated to be around 1.3 eV [59].

2. From the shape of the M^- signal and the absence of the negative parent under single collision conditions, it was deduced, that the corresponding negative ion resonance $M^{-\#}$ is generated close to the $Cl - CF_2CF_2Cl$ dissociation limit.

In addition to M^-, further negative species have been observed in the cluster experiments: Cl^- (dominant channel) , M_n^- for $(n = 1 - 4)$, solvated ions of the form $M_n{\cdot}Cl^-$ for $(n = 1 - 4)$ all peaking at 0.3 eV, solvated ions $M{\cdot}F^-$ at 1.5 eV and F^- and Cl_2^- with a yield pattern similar to that in the gas phase. The Cl_2^- generation in clusters has been observed slightly to be enhanced at higher energies, supported most likely by aggregation of the intermediate ion.

6.1.2 ESD from $C_2F_4Cl_2$ nanofilms

Interactions of free electrons with condensed $C_2F_4Cl_2$ molecules have been investigated within the framework of this thesis using *Electron Stimulated Desorption* (ESD) technique.

Thin molecular films are prepared by depositing the compound onto the gold substrate maintained at temperatures around $40 - 45$ K by a helium cryostat. Spectra are recorded under 100 nA impinging electron current with an energy resolution of about 0.3 eV. The absolute energy scale is established using the calibration procedure based on the onset of the transmitted current, defined as zero energy reference (ZER). The inspected energy range is between 0 eV and 18 eV. Because the recording time is about 25 s for a particular fragment, the $C_2F_4Cl_2$ film is exposed to ≈ 3 μC electron dosage of various energy within one scan duration.

Fig. 6.2 shows yield functions of negative ions, formed via ESD to 6 monolayers (ML) thin $C_2F_4Cl_2$ film. The ion yields in Fig. 6.2 represent the first scan from newly prepared film for every particular anionic fragment. Contrary to fragmentation observed in the gas phase (previous section), anion desorption from condensed phase is restricted to only three fragments, namely Cl^-, F^- and Cl_2^-, with ion yield intensities decreasing with irradiation time. Because of existing desorption restrictions at the surface, other fragments observed under collision free conditions may also be generated in condensed phase but remain at the surface.

Desorption of Cl^- predominantly occurs in the energy range between 7 and 12 eV, virtually not observed in DEA to gas phase $C_2F_4Cl_2$. The Cl^- desorption yield peaking at 8.3 eV is suggested to be initiated through an

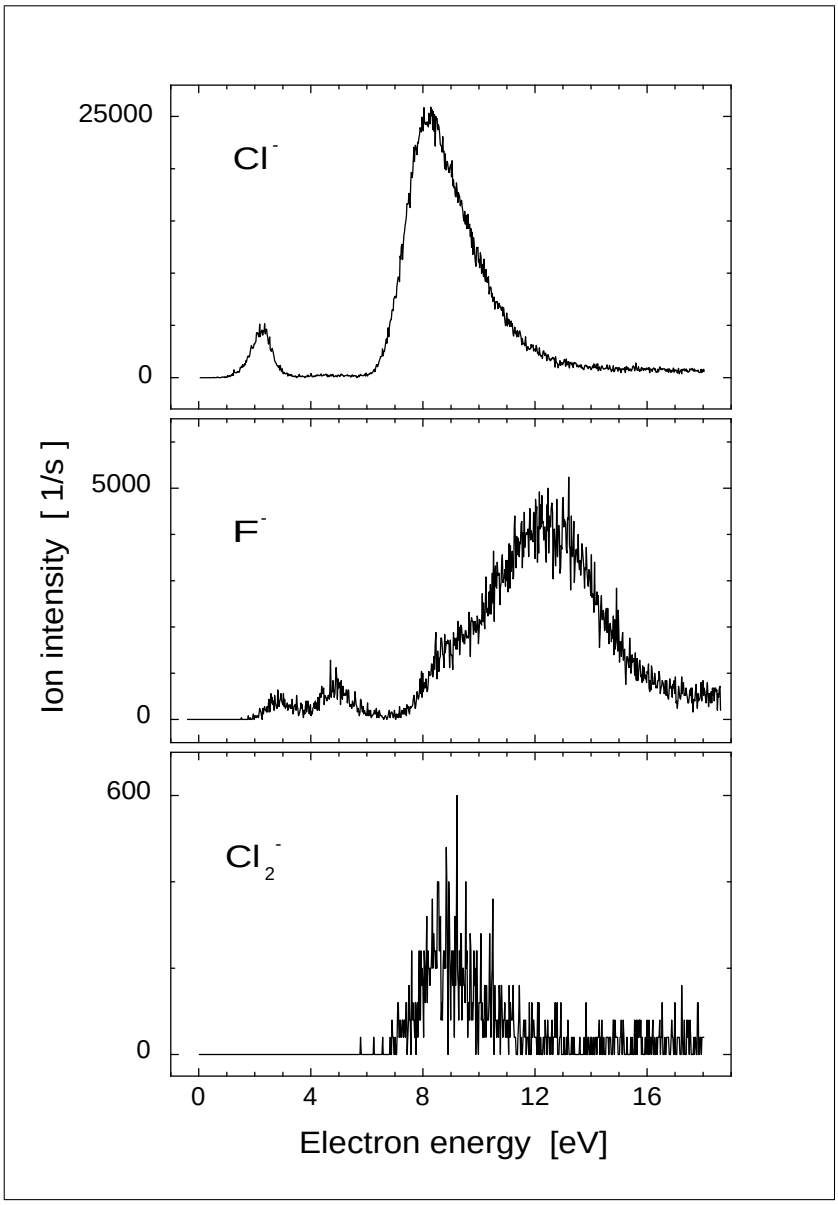

Figure 6.2: *Electron stimulated desorption of* $\mathrm{Cl}^-, \mathrm{F}^-$ *and* Cl_2^- *from 6ML thin* $\mathrm{C_2F_4Cl_2}$ *film. The spectra represent the first scan from newly prepared sample for every particular fragment.*

electronically excited intermediate ion (core excited resonance). On the other hand a small feature at around 2.3 eV is formed most probably through the second anionic precursor state involved in generation of all negative fragments in the gas phase. Under collision free conditions (but also in cluster experiments) the most efficient channel leads to formation of Cl^- ion and its corresponding radical at 0.3 eV. In the case of molecules adsorbed at the surface, there is a typical lack of very low energy features due to the kinetic energy filter activated by the medium. From DEA measurements in the gas gas phase, performed by Fenzlaff [60], it is known that Cl^- ions from the lowest lying resonance are generated with a negligible translational energy, which explains the suppression of desorption at 0.3 eV. As will be shown below, however, effective fragmentation processes take place near 1 eV (not seen in desorption) initiating the formation of Cl_2. The relative enhancement in Cl^- desorption at 8.3 eV follows the general observation in earlier electron stimulated desorption (ESD) experiments on cryogenic solids [30, 69]. Here longer lifetime of the NIR (supported by the environment) with respect to autodetachment can considerably boost the dissociation process. Also, dissociation from core excited resonances may result in more energetic fragments (due to more available energy), which improves then desorption efficiency.

The F^- yield function shows three resonances at energies 3.5 eV, 5 eV and 12.5 eV with a small shoulder close to 9 eV. The 3.5 eV peak can be formed via the same precursor state, which leads to F^- generation at 2.7 eV in the gas phase. Shift to higher energies, (*blue shift*) is considered due to insufficient kinetic energy of the generated ions to overcome the attractive polarization. On the broad feature lying between 8 eV and 18 eV, two resonances at 9 eV and 12.5 eV can be distinguished. They are attributed to the same precursor states involved in F^- formation in the gas phase, seen at 9 eV and 12 eV respectively. However, the resonance located at 5 eV can not be directly associated with any anionic states observed from gas phase $C_2F_4Cl_2$.

The fragment Cl_2^- appears close to the core excited resonant state at 8.3 eV yielding Cl^-. The intensity of Cl_2^- is much weaker compared to Cl^- and F^-. From the observed Cl_2^- ion yield it is not clear if the Cl atoms

arise from the same molecule or two parent molecules must be involved. The gas phase measurements have shown that Cl_2^- generation is possible even via electron attachment to a single molecule. Anyway, in the condensed phase, Cl_2^- may be initiated by PDIs of the generated anions or radicals. Note, in cluster measurements, relative enhancements in Cl_2^- ion yield at higher energy has also been discovered [59]. We can thus assume that secondary interactions may be involved in the observed Cl_2^- desorption according to

$$Cl^- + C_2F_4Cl_2 \rightarrow C_2F_4Cl + Cl_2^- \quad with \quad \Delta H_0 = 2.1eV \tag{6.7}$$

The reaction enthalpy was estimated using the known values of EA(Cl) = 3.6 eV, EA(Cl_2) = 2.4 eV, D($Cl - CF_2CClF_2$) = 3.4 eV and D($Cl - Cl$) = 2.6 eV. Taking into account the exothermicity of the reaction (6.1a) leading to Cl^- formation, we get the thermodynamical threshold of about 1.8 eV for the overall process (6.8) consisting of reaction (6.1a) in the first step and reaction (6.7) in the second step,

$$e^- + 2C_2F_4Cl_2 \rightarrow 2C_2F_4Cl + Cl_2^- \quad with \quad \Delta H_0 = 1.8eV. \tag{6.8}$$

As we have discussed earlier, formation of NIRs is strongly affected by the presence of the environment, which usually lowers the energy required to their generation (when compared with gas phase). However. the observed desorption resonance is the result of two opposing effects, namely polarization of the intermediate ion (red shift) and desorption of the fragments (blue shift). Using eq. (4.36) we can derive the energetic limits for Cl^-, F^- and Cl_2^- emission from the surface. We have used 1 eV for the polarization energy V_p in our estimation [31, 70]. The energetic thresholds for ion desorption are thus by about 260 meV(Cl^-), 125 meV(F^-) and 600 meV(Cl_2^-) higher than the corresponding values in the gas phase. These estimates were obtained under the following assumptions:

1. Eq. (4.36) was derived for unimolecular decomposition of the NIR into two particles at zero translational energy, without internal excitation of the fragments and no energy dissipation to the surrounding medium during the reaction. It is clear that these conditions may hardly be

fulfilled in reality.

2. Eq. (4.36) is valid if we consider the same value of the polarization energy for the solvated NIR and the negative fragments ($V_p(C_2F_4Cl_2^-) = V_p(Cl^-) = V_p(F^-) = V_p(Cl_2^-)$). However, we can expect that solvation energy will slightly vary for every particular anionic fragment.

The desorption yields seen on Fig 6.2 represent only the *relative desorption cross-sections*. The absolute values may roughly be estimated by comparing the ion yields between two different compounds with a well known absolute cross-section for one of them. However, the ion yields must be obtained under comparable conditions. The idea is similar as by DEA measurements in the gas phase, where the *absolute cross-section* for a partial DA channel is obtained by comparison with a well known electron attachment rate to SF_6 molecule at thermal incident energies [47, 59, 71].

The absolute cross-section σ_{da} for a particular DA channel yielding X^- may be derived from Lambert-Beer law as

$$Z(X^-) = I_0(1 - exp(-\sigma_{da}(X^-)nl)) \tag{6.9}$$

with $Z(X^-)$ the number of X^- ions per second, I_0 the number of electrons per second, σ_{da} the absolute DA cross-section, n the gas density and l the interaction length. When $n\sigma_{\mathrm{da}}l << 1$ the *absolute DA cross-section* in the gas phase may be estimated as follows [30]

$$\sigma_{gas}(X^-) = \frac{Z_{gas}(X^-)}{I_0 \gamma n_{gas} l} \tag{6.10}$$

The factor γ represents the probability for a generated ion to be detected and depends only on ion collecting and detection system.

Similarly to σ_{gas} determination, *absolute desorption cross-section* σ_{des} in the condensed phase may be approximated as [30]

$$\sigma_{des}(X^-) = \frac{Z_{des}(X^-)}{I_0 \gamma n_s} \tag{6.11}$$

with $Z_{\mathrm{des}}(X^-)$ number of desorbed ions per second and n_s density of molecules

at the surface. Under the assumption that I_0 and γ are comparable, σ_{des} for a particular fragment X^- may then be derived from σ_{gas} as follows,

$$\sigma_{des}(X^-) = \sigma_{gas}(X^-)\frac{Z_{des}(X^-)n_{gas}l}{Z_{gas}(X^-)n_s} \tag{6.12}$$

In present estimation of the desorption cross-section σ_{des}, gas phase cross-section $\sigma_{\mathrm{gas}}(Cl^-) = 2 \times 10^{-15}\mathrm{cm}^2$ at 0.3 eV [59] is used. In addition, the following assumptions concerning the parameters involved in gas and condensed phase ion yield are used: the $Cl^-/C_2F_4Cl_2$ in gas phase measurements was obtained under the 50 nA impact current with a base pressure 2×10^{-5} mbar in the chamber during the measurements. From the chamber volume, pumping speed and the capillary diameter used to form effusive molecular beam, the gas density inside the interaction volume has been estimated to be about 3 orders of magnitude higher than that in the chamber. This gives for a product of $n_{gas}l \approx 10^{14}$ cm^2. The density of the molecules at the surface is taken to be 10^{15} cm^{-2}, because to desorption contributes only the upper layer of the molecular film. Finally, the ion yields are normalized to the beam intensity. Substituting the above mentioned values to eq. 6.12 we have estimated the desorption cross-sections shown in Tab.6.1,

	$\boldsymbol{\sigma_{\mathrm{gas}}}$ **[cm^2]**			$\boldsymbol{\sigma_{\mathrm{des}}}$ **[cm^2]**	
Resonance	0.3 eV	8.3 eV	12 eV	8.3 eV	12 eV
$\mathbf{Cl^-}$	2×10^{-15}	2×10^{-17}	-	3×10^{-17}	-
$\mathbf{F^-}$	-	-	6×10^{-19}	-	5×10^{-18}
$\mathbf{Cl_2^-}$	-	3×10^{-19}	-	3×10^{-20}	-

Table 6.1: *Estimated absolute cross-sections for ion desorption.*

As we can see from Tab.6.1, in case of Cl^- at 8.3 eV σ_{des} is comparable to σ_{gas} at the same energy and one order of magnitude enhanced in the case of F^- at 12 eV. On the other hand, desorption cross-section for Cl_2^- is by about one order of magnitude lower than corresponding σ_{gas} at 8.3 eV. Since Cl_2^- is a relatively heavy fragment, suppression in desorption is expected. Anyway, absolute desorption cross-sections represent only lower limits of the corresponding absolute DEA cross-sections in condensed phase, since not

every dissociation event leads to desorption. Therefore partial DEA processes may even be enhanced with respect to gas phase.

However, the obtained σ_{des} values are only a very rough estimates due to the high uncertainty in the estimation of the density of molecules in the gas phase and the fact, that the detection conditions are not exactly the same in both experiments. Under these circumstances, the estimated values in Tab.6.1 should be taken with an uncertainty of about one order of magnitude.

6.1.3 ESD from $C_2F_4Cl_2$ films at different coverages

Fig. 6.3 illustrates the evolution of the Cl^- signal with the thickness of the $C_2F_4Cl_2$ film. Between coverages from 1 ML to 6 MLs the influence of induced image charge in the metallic substrate on ion desorption can be seen. Indeed, the low energy feature is totally quenched in the case of a 1 ML thin film. Here the attractive Coulombic force between the negative ion and opposite image charge dominates. Accordingly, the feature near 8 eV is affected in a similar way. Increasing the distance to the surface where the negative species are generated enhances the desorption efficiency. The desorption probability increases up to coverages of about 6 MLs. Here the induced image charge in the metal is expected to be screened by the $C_2F_4Cl_2$ spacer. Remember, the ion emission from the surface is still affected by dielectric film polarization. Decrease in ion intensity at 2.3 eV with further increase in layer amounts from 6 to 12 MLs is not clear yet. There is no simple interpretation for such a behavior and several competing events can lead to final suppression. Moreover, broadening of 8.3 eV resonance as well as shifting of its maximum position to higher energies with film thickness does not have any straightforward explanation. Even in the simplified unimolecular decomposition model, influence like image charge and medium polarization and change of orientation of the molecule at the surface with film thickness [72] act in opposing ways on ion desorption. In addition ion emission from the surface may be initiated by multiple electron scattering and PDIs of generated fragments [73].

We should note, that at coverages above 6 ML, the influence of accumulated charge on the surface plays an important role. The observed shift in current onsets between the first and second energy scan is around $0.5-0.6$ V. In

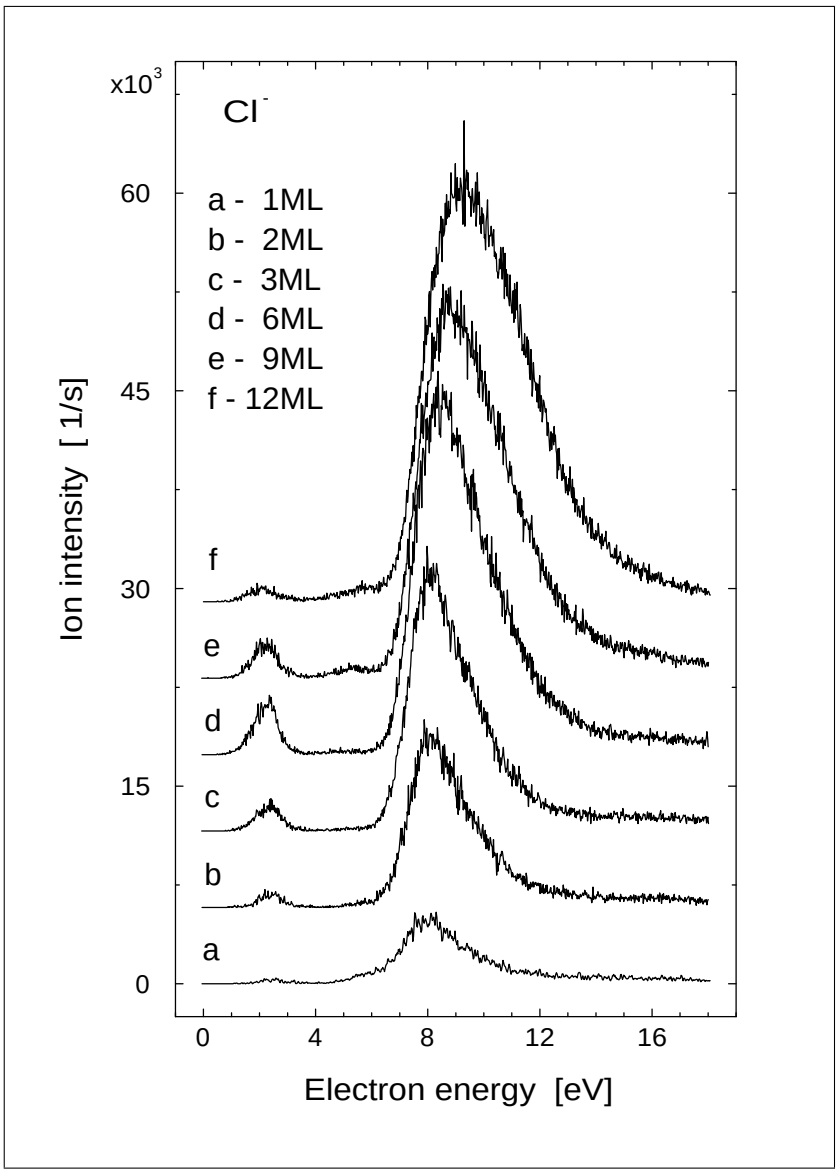

Figure 6.3: *Evolution of the Cl^- yield function with $C_2F_4Cl_2$ film thickness.*

that case incoming electrons are affected by a strong inhomogeneous electric field at the surface. This leads to a degradation of resolution of the incident beam, which increases then the uncertainty in absolute energy determination. From observed charging we can definitely expect a strong modification of the molecular solid within the recording time.

Furthermore, at higher (> 6 ML) coverages, additional intensity at the tail of 8 eV resonance can be recognized. This extra feature at 5.8 eV was attributed to Cl^- ions originating from Cl_2 molecules synthesized at the surface, (see below).

6.1.4 Electron initiated synthesis of Cl_2

Fig. 6.4 and Fig. 6.5 picture evolution of F^- and Cl^- yield functions with electron irradiation by means of successive scans. For every particular fragment, 60 successive scans have been recorded. One scan takes about 30 s in time and electron beam intensity is about 120 - 100 nA within the energy range $0 - 18$ eV.

As we can see from Fig 6.4, the difference in F^- ion yield between the first and sixtieth scan exhibits only a gradual increase in ion intensity at 12.5 eV with a suppression of the lower lying peaks at 3 eV and 5 eV. However, within the first five energy scans, the second resonance shows an increase in its intensity with a shift to lower energies (from 5 eV to 4 eV) at the same time. The explanation of these shifts is by no means straightforward, as they may result from surface charging and chemical reactions at the surface.

In contrast to F^- the Cl^- yield function shows dramatic change in its pattern with the number of energy scans. On Fig 6.5 the evolution of a new feature at 5.8 eV (*red part of the curve*) with increasing number of scans can be seen. Note the drastic increase in its intensity within the short irradiation time (60 scans $\approx$ 30 mnin). After 60 scans the peak at 5.8 eV is a dominant feature in the Cl^- spectrum. At the same time, the decrease in ion intensity at 8.3 and 2.3 eV can be seen. The evolution of 5.8 eV feature indicates that new chemical species with a high desorption cross-section is formed at the surface.

To establish the origin of this new feature we refer to earlier results from

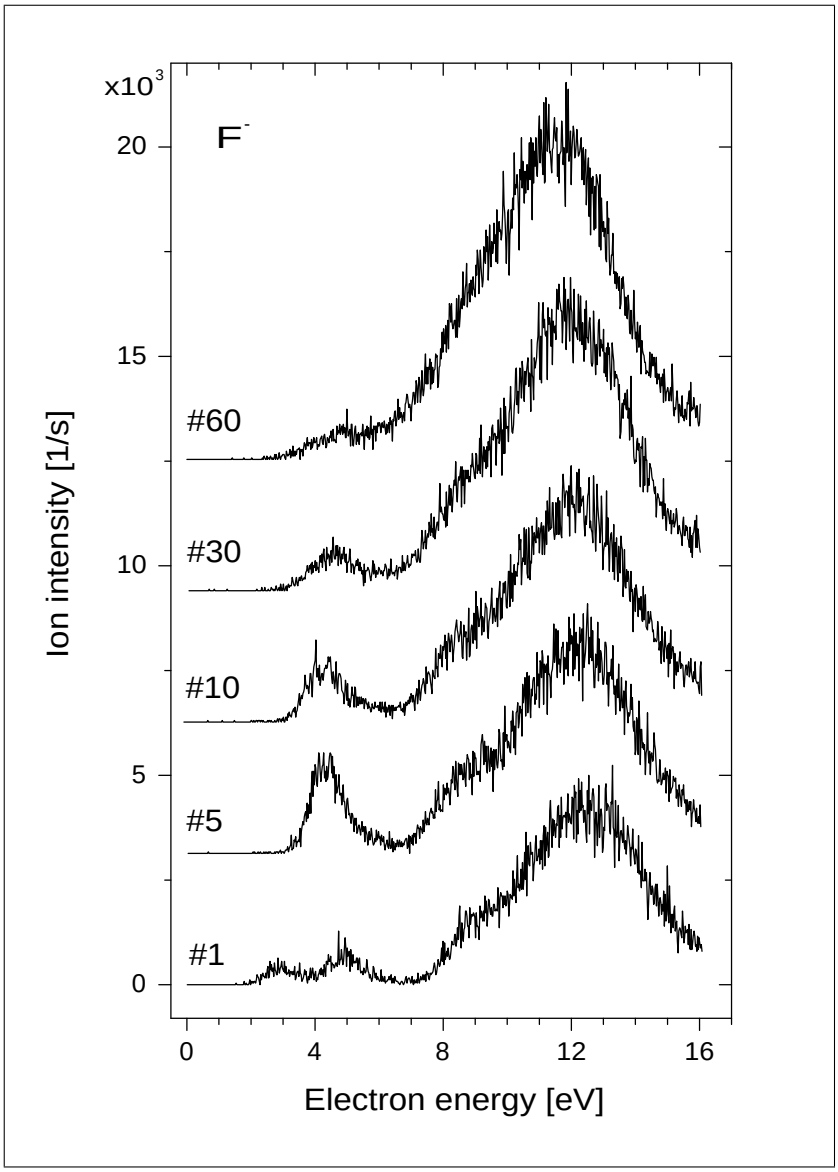

Figure 6.4: *Evolution of F^- with number of successive scans (#1 - first, #5 - fifth, ..., #60 - sixtieth scan at electron beam intensity of ≈ 100 nA and scan duration ≈ 30 s).*

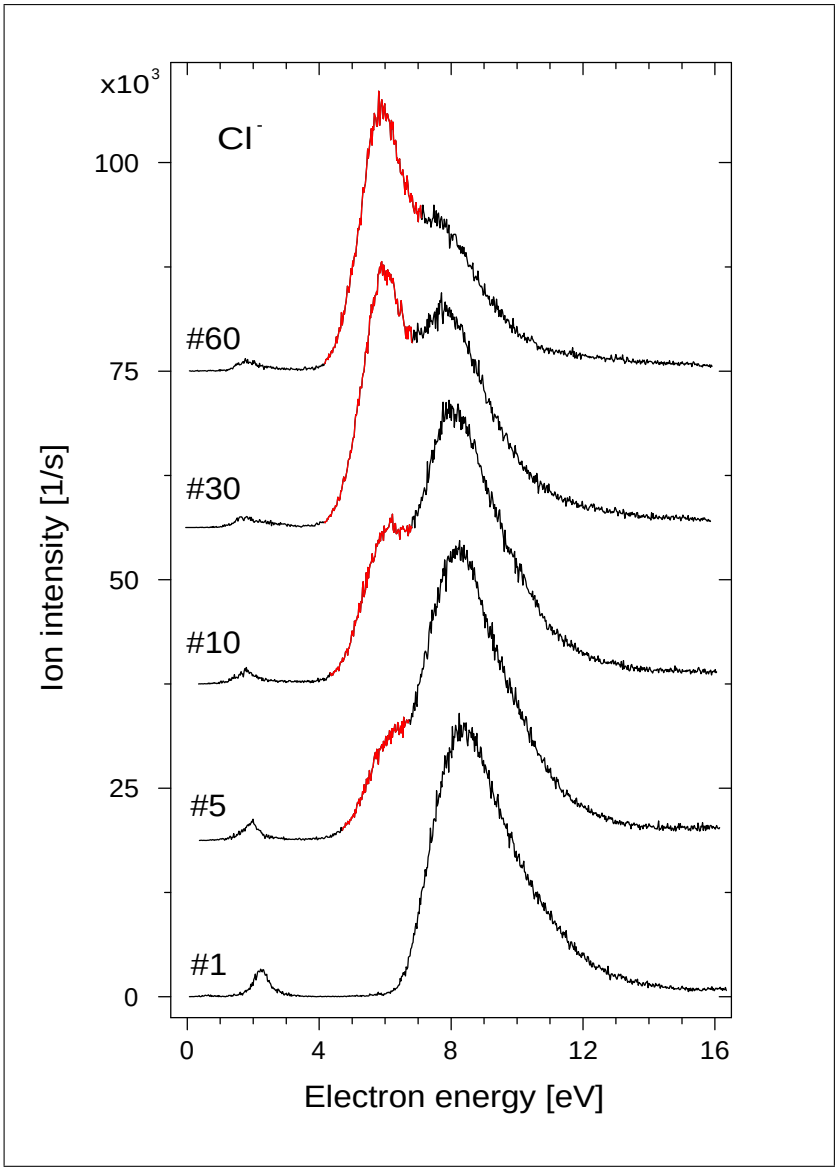

Figure 6.5: *Evolution of Cl^- with number of successive scans (#1 - first, #5 - fifth, ..., #60 - sixtieth scan at electron beam intensity of ≈ 100 nA and scan duration ≈ 30 s). Red part of the ion yields represent ESD of Cl^- from Cl_2 molecules, formed on top of the film.*

electron attachment experiments on CF_2Cl_2, performed by Hedhili *et al.* [35]. They have shown that after the irradiation of CF_2Cl_2 solids with electrons, a new intensity at 5 eV appears in Cl^- yield function. This new feature was attributed to Cl^- from Cl_2 molecules formed at the surface as was demonstrated by the difference in thermal stability between the Cl_2 and CF_2Cl_2 cryogenic films, see below (we have applied the same procedure with $C_2F_4Cl_2$ molecule) and by analyzing the kinetic energy of desorbing ions. It was found that kinetic energy distribution of Cl^- ions ejected at 5 eV from irradiated CF_2Cl_2 film fits exactly to that obtained for Cl^- ions desorbing from pure Cl_2 film at the same energy (associated with $^2\Pi_u$ core excited Cl_2^{-*} resonant state [74]). We should note that corresponding ions have been found to desorb with appreciable kinetic energy, increasing linearly with primary energy [35,74]. This may explain the difference in peak position between the experiments *i.e. new feature at* 5 *eV from* CF_2Cl_2 *compared to peak appearing at* 5.8 *eV from* $C_2F_4Cl_2$ *measured in our laboratory.* The peak position can vary according to the detection efficiency of the ion collecting system. In systems with a stronger discrimination against energetic ions, the peak in the desorption spectrum will appear at lower energies and *vice versa.* To prove that the 5.8 eV feature originates from Cl_2, desorption spectra from pure Cl_2 film have been recorded in our laboratory. We have observed that under our detection conditions, Cl^- intensity attributed to $^2\Pi_u$ resonant state appears near 6 eV and is thus shifted to higher energies with respect to desorption resonance from pure Cl_2 film observed by Azria [74].

Cl^- yields from pure Cl_2 film (red curve) and irradiated $C_2F_4Cl_2$ solid (black curve) are shown on Fig.6.6. For the better visualization, the ion intensity coming from a thin molecular film of chlorine at 5.8 eV is scaled by a factor β to that of 5.8 eV feature. As we can see, both features fit exactly (their position and shape).

The Cl_2 synthesis at the surface is also demonstrated by the difference in thermal stability between the $C_2F_4Cl_2$ and Cl_2 molecular films. According to our conditions in the chamber (base pressure 10^{-10} mbar), the $C_2F_4Cl_2$ film evaporates above 100 K, while the molecular chlorine evaporates at 75 K. The stability of the Cl_2 layer (formed after the irradiation) is then studied

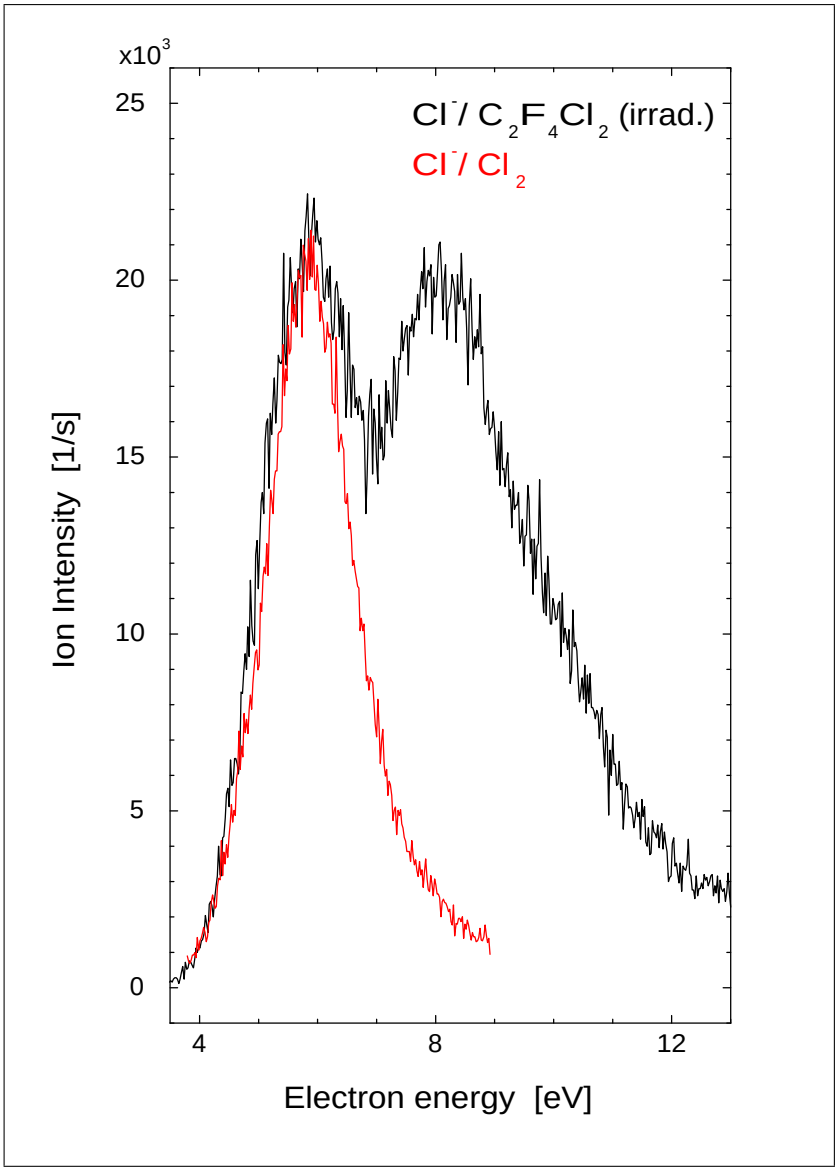

Figure 6.6:
black curve - Cl^- ion yield from irradiated $C_2F_4Cl_2$ sample (10 eV, 100 nA, 240 s),
red curve - Cl^- ion yield from pure Cl_2 film, scaled by factor β to that from irradiated $C_2F_4Cl_2$ at 5.8 eV.

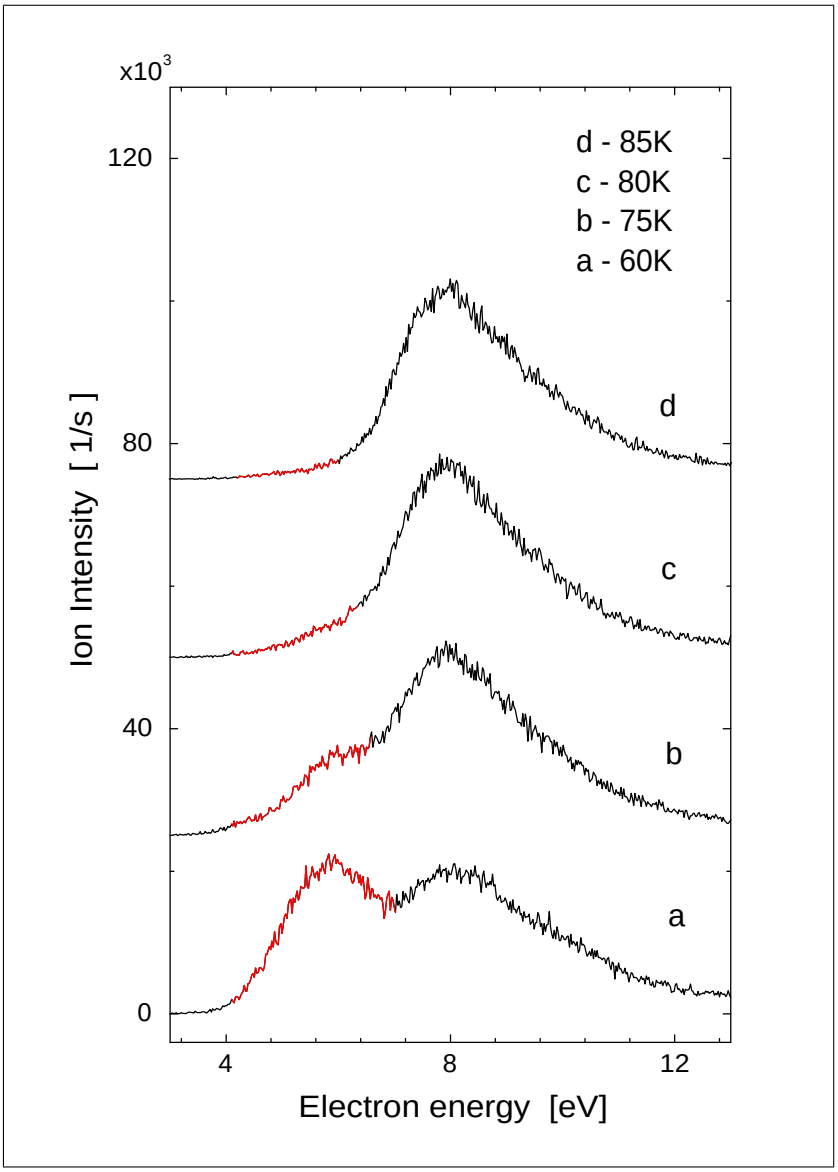

Figure 6.7: *Cl^- ion yield from irradiated $C_2F_4Cl_2$, (10 eV, 100 nA, 240 s) - temperature dependency (explanation see text).*

by monitoring the Cl^- desorption at different sample temperatures, Fig. 6.7. The temperature of the sample was established within $\pm$ 5 K accuracy in the energy range $60 - 100$ K. As a reference point the boiling temperature of nitrogen at 77 K was used for calibration. The measurement procedure consists of the following steps: at first, the molecular film is exposed to the electron beam for about 240 s, at 10 eV electron energy and 100 nA beam intensity. The irradiation proceeds at 45 K sample temperature. Afterwards the sample is heated to a particular temperature and Cl^- desorption spectrum is recorded. For every given temperature the procedure is repeated with a newly prepared film. We have then observed that heating the sample up to 60 K does not induce any changes in the overall Cl^- yield function. However, above that temperature the contribution of Cl^- intensity at 5.8 eV decreases. The 5.8 eV feature vanishes after heating the sample to 85 K, which is explained by evaporation of the Cl_2 layer. Finally, increasing the sample temperature above 100 K shows decrease in ion intensity at 8.3 eV, attributed to evaporation of $C_2F_4Cl_2$ film, (not shown here).

All the above described observations unambiguously show that Cl_2 molecules are synthesized at the surface. To summarize, the appearance of the 5.8 eV intensity may be interpreted as follows. The interaction of low energy electrons with the film of $C_2F_4Cl_2$ molecules initiates production of the molecular chlorine via primary and/or secondary reactions. DEA to Cl_2 then results in desorption of Cl^- ions at 5.8 eV of primary electron energy. In order to understand the origin of the reactions, further investigations have been performed, see below.

6.1.5 Electron energy dependence of Cl_2 formation

As mentioned above, Cl_2 formation from CF_2Cl_2 has already been studied by Hedhili. However, due to technical reasons, the energy dependence of the reaction was investigated only down to 5 eV of primary energy [35]. In our experiment with condensed $C_2F_4Cl_2$ molecules, we have extended the investigations down to electron energies of about 1 eV. Moreover, we have used much higher beam intensities, which enables to study the completion of the reaction within a reasonable time.

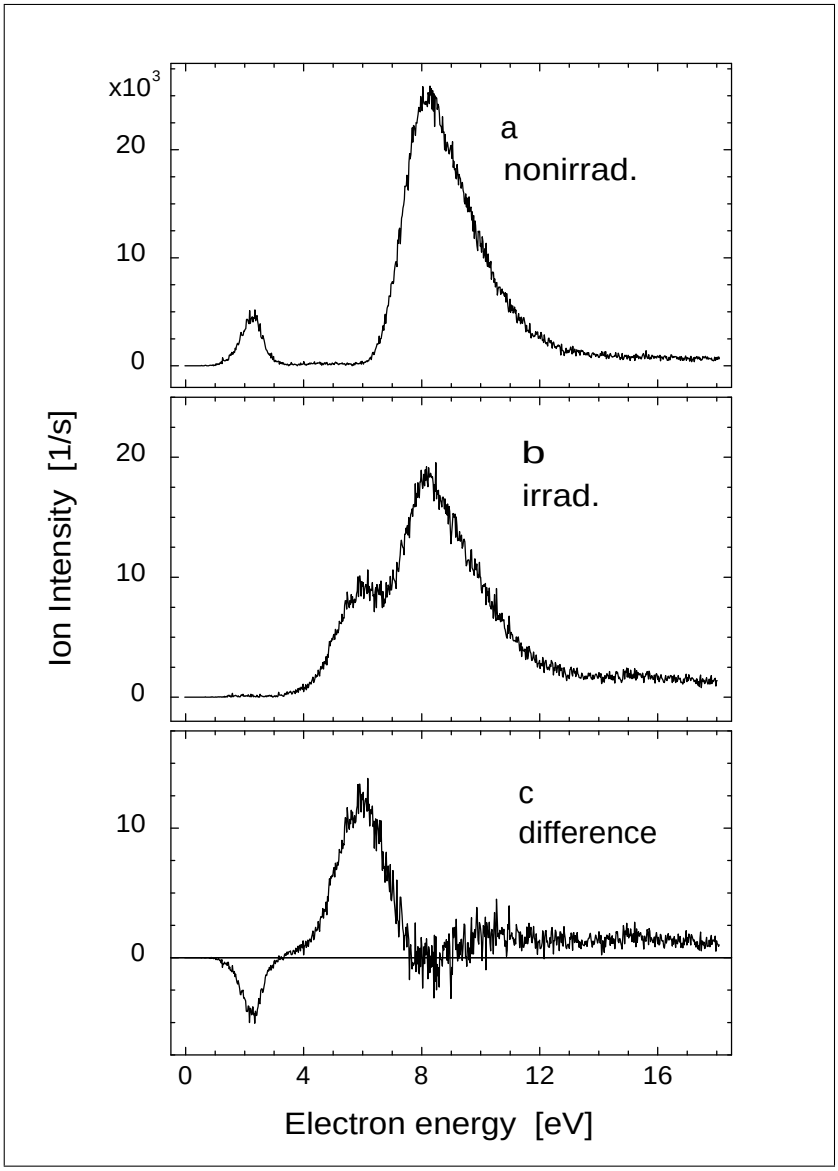

Figure 6.8: *Cl^- yield function from 6 ML thick $C_2F_4Cl_2$ film*
a) *before irradiation*
b) *after irradiation at 9 eV for 120 s*
c) *difference spectrum (c)=γ(b)-(a) after normalization of b) to a) at 8.3 eV by scaling factor γ.*

In order to reveal some information on the dependence of Cl_2 formation on primary electron energy, a 6 ML thin molecular film of $C_2F_4Cl_2$ was exposed to the electron beam stepwise at different energies but comparable dosages. On Fig. 6.8 the difference between the irradiated sample b) and nonirradiated sample a) after the normalization is shown. The ion yield from the first energy scan represents that for the nonirradiated sample. The recorded ion yield from the irradiated sample is then obtained after bombardment of the newly deposited $C_2F_4Cl_2$ film at a defined electron energy and dosage (120 s, $\approx$ 100 nA). The normalization procedure consists of scaling the irradiated ion yield `(b)` to that of nonirradiated `(a)` at 8.3 eV by a factor γ. The difference spectrum `(c)` is the result of γ`(b)-(a)`, Fig 6.8 c). The area of the resulting signal between 4 and 8 eV is assigned as *relative reaction cross-section for Cl_2 formation* at a particular energy. The procedure is then stepwise repeated at different electron energies, in each case with a newly deposited film, resulting in an energy dependence of the *reaction cross-section* pictured on Fig 6.9 a). For the accuracy of the evaluated data the following points have to be noted:

- The energy is assigned according to energy calibration after irradiation, but in the course of irradiation the electron energy shifts due to charge accumulation at the surface. The obtained charging at a particular energy is measured by a shift in the current onset ΔV, Fig 6.9 b). The figure shows, that the charging effect is more pronounced at low impact energies ($<$ 2 eV), which reflects the high attachment cross-section of the molecule at lower energies as well as the fact that desorption of anionic fragments is not operative in this energy region. Also the time evolution of film charging at 9.5 eV irradiation energy is inserted in Fig 6.9 b). It can be seen that the ΔV value changes considerably within the first 30 s of irradiation and tends to saturate with increasing the time. The electron impact energy is thus well defined after an irradiation time of about 2 min. However, to correct for the time evolution of charging, the data points in Fig 6.9 a) should be shifted by about 0.2 V to higher energy. Of course, in the low energy domain the film charging is more abundant and the energy shift may be slightly higher.

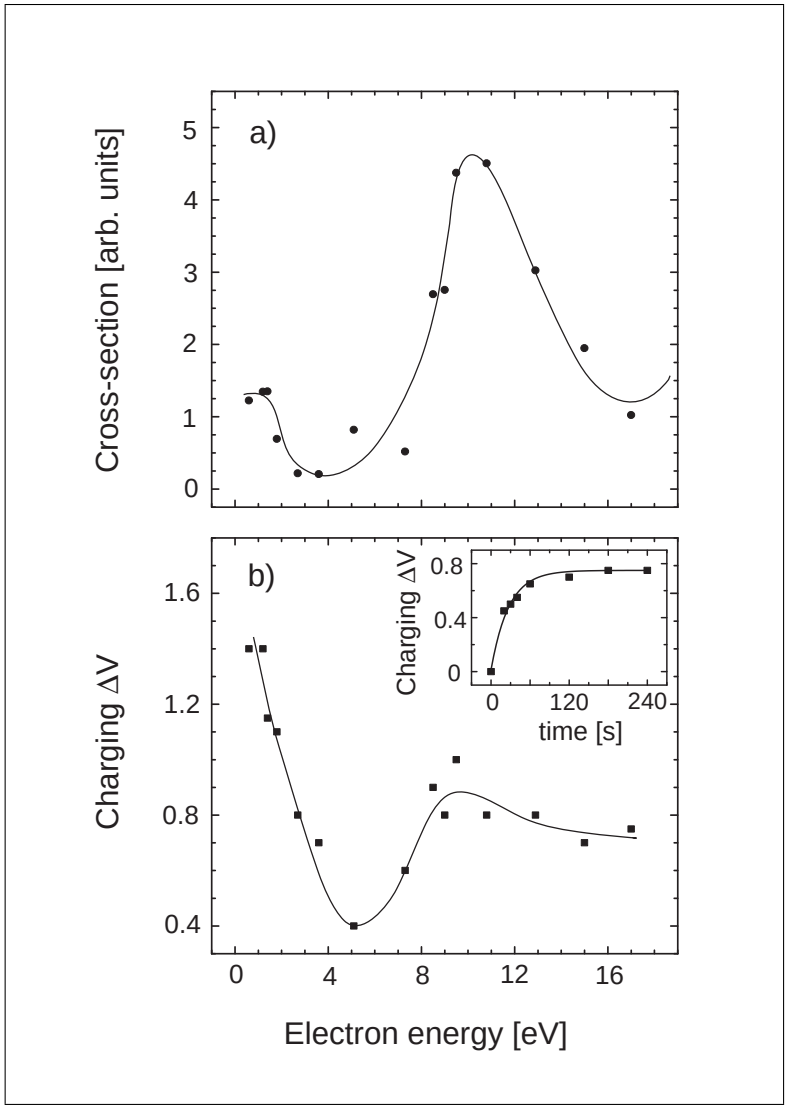

Figure 6.9:
a) *energy dependence of the relative cross section for Cl_2 formation. The numbers represent the peak area of the contribution at 5.8 eV assigned to Cl^- from Cl_2 after irradiation for 120 s each time.*
b) *shift of the onset of the injection current (ΔV) with respect to the monochromator potential after 120 s irradiation; insert: time evolution of charging at 9 eV irradiation.*

- For the evaluation of the area in the difference spectrum, Fig 6.8 (c) uncertainty due to ion intensities have to be considered. The ion intensity can vary with film thickness and sample position when recording the ESD spectra, as we used newly deposited film for every particular energy. Accordingly, the overall error due to additional electron dosage (30 s, $\approx$ 100 nA) at various energies by probing the results should be included. The scattering of data in Fig. 6.9 a) may be then considered as a measure of the uncertainty stated by the measurement and analyzing procedure.

- The reaction cross-section pictured on Fig. 6.9 a) may slightly be modified due to different impact electron densities. The irradiated region strongly depends on magnetic field strength, electron beam intensity and energy. For a typical measurement conditions (B = 30 Gauss, I = 120 nA) the irradiated area changes from 0.1 to 0.05 cm^2 in the energy range from 0 to 20 eV (obtained from the determination of the beam profile at different electron energies). Since the desorption intensity (recorded in order to establish the amount of Cl_2 molecules formed at the surface) strongly depends on the concentration of molecules at the surface, sample irradiation at different energies should proceed in the way that electron dosage per unit area is the same. Despite the dependence of the irradiated area on primary electron energy, charge accumulation at the surface tends to spread the incoming electron beam. These effects tend to underestimate the reaction cross-section at low energy (by factor of less than 2 estimated for the relevant energy range)

Apart from the mentioned uncertainties in the relative cross-section values, Fig 6.9 a) clearly shows the dependence of Cl_2 formation from the primary electron energy. Noticeable is, that the reaction is operative at energies below the first electronically excited state of the molecule (< 3 eV). Furthermore, we can see that the reaction cross-section shows a resonant character and drops almost to zero at 4 eV electron impact energy.

Remember that the cross-section values were obtained after a short time irradiation ($\approx$ 2 min). As will be shown below, the extend of the reaction (ra-

tio of concentration $Cl_2/C_2F_4Cl_2$) depends on the electron dosage. However, for a sufficiently high dosage the result is considerably different when comparing the irradiation at subexcitation energies with that at energies above the threshold of electronic excitation .

6.1.6 Proposed mechanisms of Cl_2 formation

As can be seen from Fig 6.9, the energy dependence of the Cl_2 formation shows a resonant character and follows qualitatively the energy dependence of $Cl^-/C_2F_4Cl_2$ desorption and charge accumulation at the surface. The reaction is obviously more effective around 10 eV as well as below 3 eV incident energy. While at higher energies different reaction routes including electronically excited states may be involved, at energies below 3 eV only DEA to $C_2F_4Cl_2$ may activate Cl_2 formation, either via *direct unimolecular reactions* or *indirect secondary reactions*.

Considering *direct unimolecular reactions*, the following processes can contribute,

$$e^- + C_2F_4Cl_2 \rightarrow C_2F_4Cl_2^{\#-} \rightarrow C_2F_4^- + Cl_2 \quad with \quad \Delta H_0 < 2.9\ eV \tag{6.13a}$$

$$e^- + C_2F_4Cl_2 \rightarrow C_2F_4Cl_2^* + e^- \rightarrow C_2F_4 + Cl_2 + e^- \quad with \quad \Delta H_0 = 2.9\ eV \tag{6.13b}$$

In both reactions the Cl radicals originate from different C atoms within the same parent molecule. The reaction (6.13a) proceeds via formation of the NIR, while in the second reaction an electronically excited neutral precursor state is involved (6.13b). However for the (6.13b) channel one would not expect a resonant behaviour and it may therefore be excluded as the major pathway for Cl_2 production. Furthermore, the reaction enthalpy of (6.13b) is about 2.9 eV (estimated using known enthalpies of formation for $C_2F_4Cl_2$ and C_2F_4, see Tab. 6.2) and would not contribute to Cl_2 synthesis in the low energy region.

The reaction channel (6.13a) has not been observed neither in the gas phase nor in the cluster measurements. Anyway the $C_2F_4^-$ does exist in the gas phase, as was observed in electron attachment to perfluoroethene clusters

[2]. Therefore the reaction (6.13a) can not be excluded in Cl_2 formation in condensed phase. Since C_2F_4 may not possess sufficient electron affinity (value is expected to be near 0 eV [75, 76]) to drive the reaction at 1 eV it is most likely that reaction (6.13a) only has a minor contribution to the final reaction cross-section.

Contrary to $C_2F_4^-$, Cl_2^- was observed via reaction (6.3), which is the complement to reaction (6.13a). In order to form a neutral Cl_2 molecule, electron transfer from Cl_2^- to the metal or to the molecules in the vicinity must take place. This is, however, very unlikely process because of the considerable electron affinity of Cl_2.

In summary, *direct unimolecular processes* can be excluded to be responsible for observed behaviour of the *reaction cross-section* on Fig 6.9a) and we assume that *secondary reactions* must be involved.

Secondary reactions involve post dissociation collisions of the products generated via primary electron-molecule interactions. For simplicity we will not analyze further reactions induced by electron scattering on these products.
One of the route leading to Cl_2 formation is by recombination of two Cl radicals generated by two unimolecular processes. The Cl radicals may also be formed through the resonance or an electronically excited neutral,

$$e^- + C_2F_4Cl_2 \rightarrow C_2F_4Cl_2^{\#-} \rightarrow C_2F_4Cl^- + Cl \tag{6.14a}$$

$$e^- + C_2F_4Cl_2 \rightarrow C_2F_4Cl_2^* + e^- \rightarrow C_2F_4Cl + Cl + e^- \tag{6.14b}$$

Reaction (6.14a) was observed in the gas phase as a weak signal with an appearance energy close to 0.5 eV. In the gas phase Cl radicals are expected to be generated with negligible kinetic energy, but due to lower energy for Franck-Condon transitions to form a NIR in the condensed phase, the radicals generated at 1 eV can gain sufficient translational energy to be mobile at the surface and form moleculecular chlorine. Reaction (6.14a) may thus be involved in Cl_2 formation in the low energy regime. Although $C_2F_4Cl^-$ was not observed in the gas phase at higher energies, one can expect that the reaction is operative in the condensed phase. In the condensed phase, the

desorption of heavy polyatomic fragments is very unlikely, therefore we could not really prove the existence of this channel using ESD measurements.
On the other hand the reaction (6.14b) can only contribute to Cl_2 formation at higher energies since it involves electronically excited state of the parent molecule. Similarly to reaction pathway (6.13b), it is not expected for this channel to show a resonant character of the reaction cross-section.

The overall reaction initiated by (6.14a) and proceeding through Cl recombination at subexcitation energies can then be expressed as

$$2e^- + 2C_2F_4Cl_2 \rightarrow 2C_2F_4Cl^- + Cl_2 \quad with \quad \Delta H_0 < -1.5\ eV \tag{6.15}$$

A further possible reaction concerns the interactions of Cl^- ions and/or C_2F_4Cl radicals generated via DEA to $C_2F_4Cl_2$ with surrounding molecules, reaction (6.1a). The possible scenario for Cl_2 formation may then proceed via interaction of Cl^- with $C_2F_4Cl_2$ or by recombination of C_2F_4Cl radicals generated via two unimolecular reactions,

$$\begin{aligned} e^- + C_2F_4Cl_2 \quad &\rightarrow \quad C_2F_4Cl + Cl^- \\ & \qquad Cl^- + C_2F_4Cl_2 \rightarrow C_2F_4Cl^- + Cl_2 \qquad (6.16) \\ & \qquad C_2F_4Cl + C_2F_4Cl \rightarrow C_4F_8 + Cl_2 \qquad (6.17) \end{aligned}$$

The reaction enthalpy of (6.16) is estimated to be less then 1.9 eV. Since the Cl^- ions formed in the first step are generated with some excess energy at 1 eV, it is very probable that the reaction is operative at impact energies down to 1 eV. The overall process can then be expressed as

$$e^- + 2C_2F_4Cl_2 \rightarrow C_2F_4Cl + C_2F_4Cl^- + Cl_2 \quad with \quad \Delta H_0 < 1.45\ eV \tag{6.18}$$

The C_4F_8 formed in (6.17) can represent cyclobutane or an isomer of butene and the overall process is then expressed as

$$2e^- + 2C_2F_4Cl_2 \rightarrow 2Cl^- + cC_4F_8 + Cl_2 \quad with \quad \Delta H_0 = -0.7\ eV \tag{6.19}$$

when considering formation of cycloperfluorobutane as the most stable C_4F_8

[77]. For perfluorobutene isomers, the reaction would be endothermic by more than 5 eV or would result in formation of $C_4F_8Cl_2$. Since reaction (6.19) follows the Cl^- dissociation pathway and is operative at subexcitation energies, we suggest that it is essentially involved in Cl_2 formation. All reaction enthalpies represent gas phase values and were estimated using the established data summarized in Tab. 6.2.

	EA(X)[eV]	**ΔH_f(X)[kJmol^{-1}]**
Cl	3.6	121.3
F	3.4	79.4
Cl_2	2.4	0
C_2F_4	near 0 eV	−659
c-C_4F_8	0.6	−1488
C_2F_4Cl	2.9[a]	−730[b]
$C_2F_4Cl_2$	1.3[a]	−937

Table 6.2: *Electron affinities (EA) and enthalpies of formation (ΔH_f) used to establish the reaction enthalpies ΔH_0. Data taken from [68], [77] and [78].*
[a] *lower limit estimated by Langer et. al [59].*
[b] *established using $\Delta H_f(C_2F_4Cl_2) = -937\ kJmol^{-1}$, $\Delta H_f(Cl) = 121\ kJmol^{-1}$ and $D(Cl - CF_2CF_2Cl) = 3.4 \pm 0.1\ eV$.*

Irrespective of the detailed sequence of the reaction, Cl_2 formation at subexcitation energies implies that dissociative electron attachment must be the initial step, as the only reaction operative in this energy regime. Out of the above described secondary processes, reactions (6.15),(6.18) and (6.19) may take place below 3 eV and may thus be involved in observed Cl_2 formation at that energy. In order to establish to what degree primary or secondary reactions as well as multiple electron collision events contribute to formation of molecular chlorine at the surface, further investigations of the reaction under varying $C_2F_4Cl_2$ concentration (see later) and electron beam intensity must be performed.

6.1.7 Complete chemical transformation of a molecular film at subexcitation energies

We have further investigated Cl_2 formation at different incident energies but with increased electron dosages up to several mC (corresponding to an irradiation time up to about 20 hours). The energy dependence of the reaction rate on Fig 6.9a) indicates that DEA is involved in Cl_2 formation. The DEA to $C_2F_4Cl_2$ definitely initiates the reaction at subexcitation energies as the only operative process. At higher impact energies electronically excited parents and resonances may be involved, which makes the identification of the relevant reactions more complicated. The results from extended irradiation show that at energies above the electronic excitation threshold, irradiation leads to some equilibrium between the initial molecule ($C_2F_4Cl_2$) and the products (Cl_2 plus some byproducts) accompanied with an overall degradation of the sample. The film bombardment at 4 eV, where the reaction cross-section is very weak, results in an equilibrium appreciably on the side of the initial molecule with only a moderate overall degradation. On the other hand, we have found that the initial molecular film consisting of $C_2F_4Cl_2$ molecules can be completely transformed to Cl_2 molecules plus some byproducts when using the electrons at subexcitation energies. In order to make a complete chemical transformation at the surface one needs a tool which acts on the initial molecules and initiates the reaction but does not affect the generated products. In the following we will show that low energy electrons are such a tool for the investigated system.

Fig. 6.10 demonstrates the evolution of Cl^- desorption during bombardment of the molecular $C_2F_4Cl_2$ film with electrons at 9.5 eV. The beam intensity during the bombardment varies between 40 and 50 nA. For the calculation of the electron dosage, the average value was used. The beam resolution is about 0.2 eV at 50 nA intensity but detoriates with charge accumulation at the surface. During irradiation the energy of the electron beam is kept constant, but probing desorption scans (scan time 25 s corresponding to a dosage of about 1 μC and of various electron energy $0 - 16$ eV) are taken every hour. Between two probing scans the molecular film is exposed

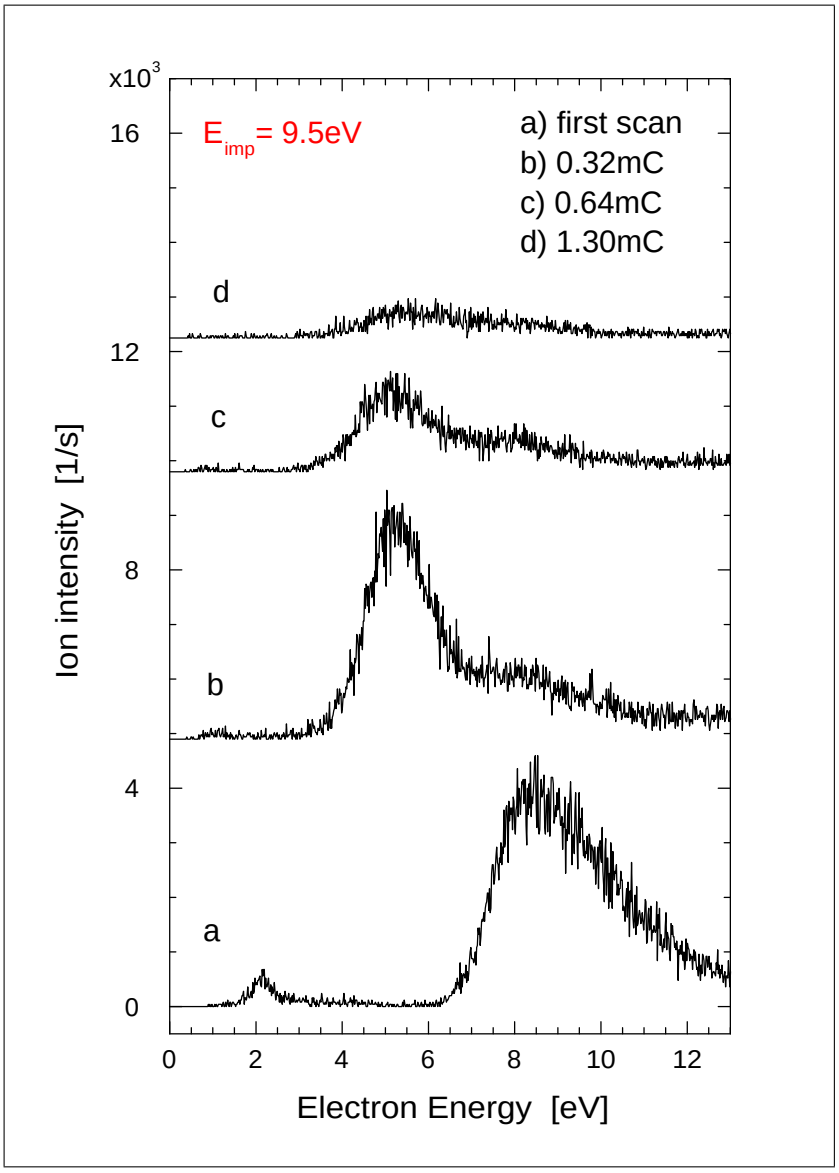

Figure 6.10: *Evolution of Cl^- desorption from a 6 ML $C_2F_4Cl_2$ film. The Cl^- ion yields are obtained after sample irradiation with electrons at 9.5 eV of given dosages.*

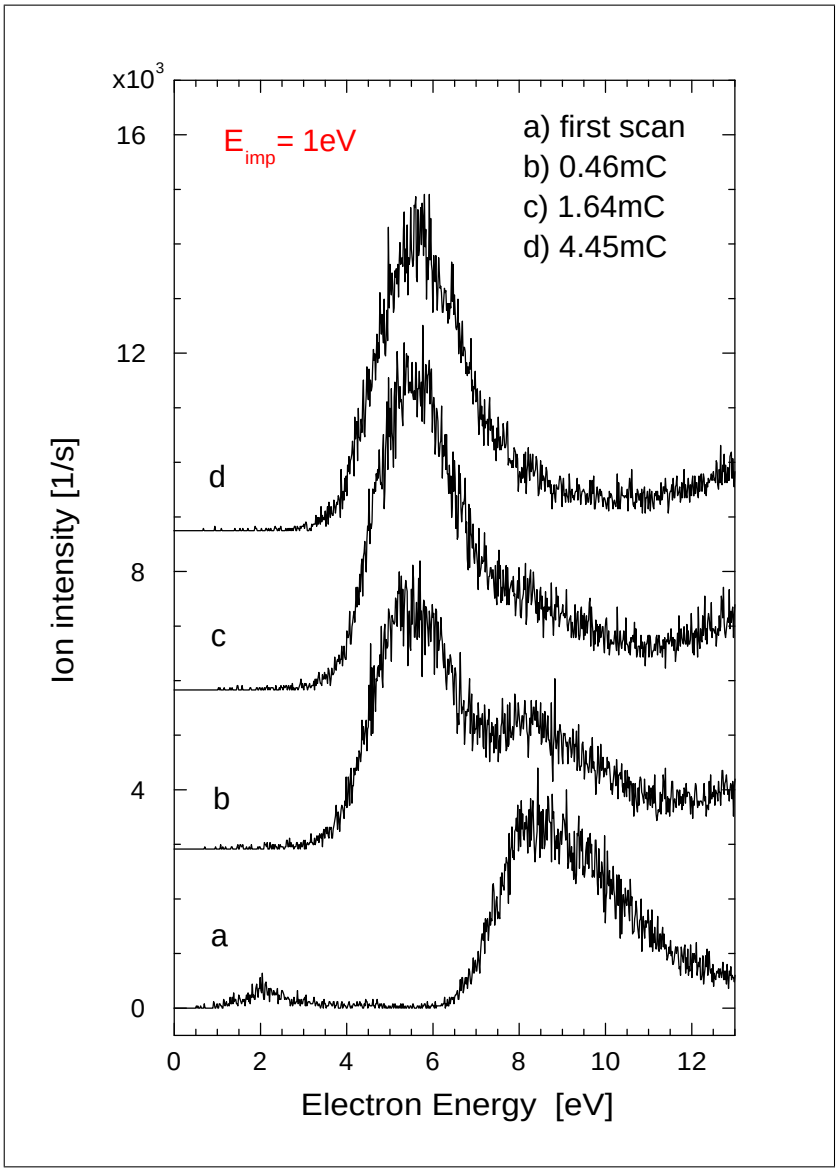

Figure 6.11: *Evolution of Cl^- desorption from a 6 ML $C_2F_4Cl_2$ film. The Cl^- ion yields are obtained after sample irradiation with electrons at 1 eV of given dosages.*

to an electron beam of defined energy with a dosage of about 0.16 mC. The influence of the probing scans to the final results is therefore minimal. From Fig. 6.10 we can see that irradiation at 9.5 eV leads to Cl_2 formation at the surface (shown by the appearance of 5.8 eV peak) followed by degradation of the $C_2F_4Cl_2$ feature (at 8.3 eV) at the same time. We have found, that some equilibrium between the initial molecule $C_2F_4Cl_2$ and the product Cl_2 is achieved within the first 5 min of irradiation (not shown on the figure). Further increase of electron dosage leaves the ratio between these two features unaffected but leads to the overall degradation of the molecular film, caused most likely by material evaporation from the irradiated area.

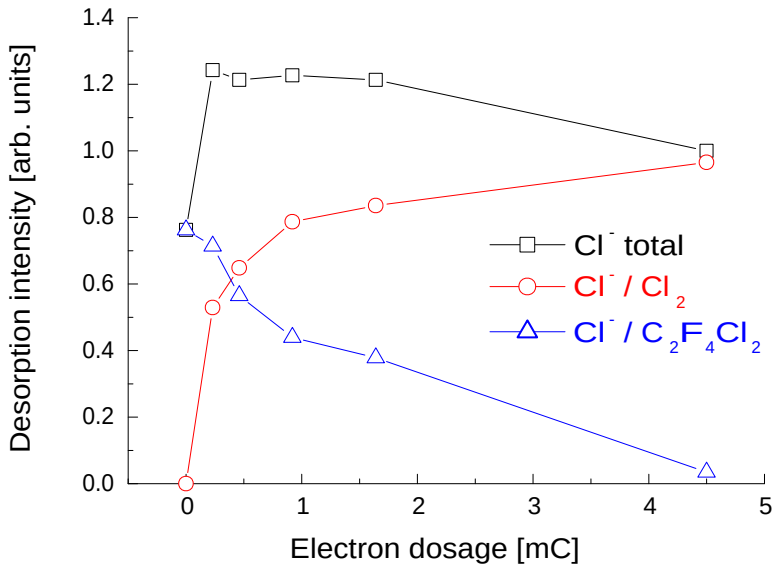

Figure 6.12: *Progress of the film transformation in the course of its irradiation at* 1 *eV electron energy. The points in the figure are assigned in the following way:*
△*:area of* 8.3 *eV peak as a measure of initial molecule at the surface*
O:area of 5.8 *eV peak representing the amount of* Cl_2 *molecules formed at the surface*
□*:total desorption area between* 4.5 *and* 12 *eV energy*

Upon irradiation with electrons at 1 eV the situation changes considerably, Fig. 6.11. Here, the irradiation leads as well to Cl_2 formation. However, film exposure to an electron dosage of about 4.45 mC (corresponding to an

irradiation time of about 19 hours) results in a desorption yield peaking at 5.8 eV, which is a nearly perfect image of the desorption resonance obtained from a pure Cl_2 layer. Furthermore there is no indication of the presence of $C_2F_4Cl_2$ molecules at the surface. We thus assume that using electrons at subexcitation energies we modify the molecular film in the way that the initial $C_2F_4Cl_2$ molecules are transformed into Cl_2 molecules with some perfluoro compounds as byproducts as discussed above. The total transformation is quantitavely demonstrated on Fig. 6.12. The figure illustrates the progress of the reaction with increasing the electron dosage in terms of the area of the total desorption intensity ($\square$) and that area due to $C_2F_4Cl_2$ at the surface ($\triangle$) as well as due to Cl_2 synthesized after irradiation (O). The corresponding values were obtained in the following way. The total intensity represents the integral value of the ion yield from irradiated film in the energy range from 4 to 12 eV, Fig. 6.13. As a measure of the initial molecule at the surface, the integral of 8.3 eV intensity in the energy range from 6 to 12 eV was used. The area was estimated using the first desorption scan scaled by a factor γ to that intensity from the irradiated sample at 8.3 eV. The difference between the ion yield from the irradiated film and scaled first scan gives an 5.8 V resonance. The integral of this feature between 4 and 8 eV energy is then assigned as a measure of Cl_2 molecules formed at the surface.

The initial increase in total intensity on Fig. 6.12 is due to higher desorption cross-section for Cl^-/Cl_2 compared to that for $Cl^-/C_2F_4Cl_2$, which was also expected from the energy distribution analysis. The figure also shows only a moderate decrease in the overall intensity, caused probably by the contamination of the surface with a residual gas during the long time irradiation and also be the desorption of neutral molecules.

From the figure it is clear, that the initial $C_2F_4Cl_2$ molecule is efficiently decomposed at 1 eV with increasing the electron dosage. Moreover, there is no indication of its presence at the surface after the dosage of about 4.45 mC. Contrary to it, the amount of Cl_2 molecules formed at the surface is rising and tends to saturate at higher dosages. The data points in the figure are normalized with respect to final Cl^-/Cl_2 feature obtained after the irradiation (4.45 mC).

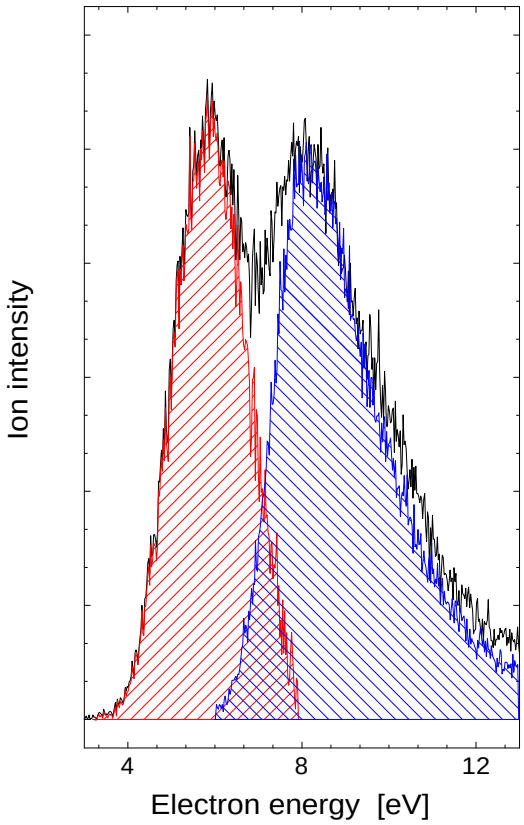

Figure 6.13:
black curve *- ion yield from irradiated $C_2F_4Cl_2$ sample.*
blue curve *- ion yield from the first scan with intensity scaled by a factor γ to that of irradiated at 8.3 eV.*
red curve *- represents the Cl^-/Cl_2 obtained as a difference between irradiated and scaled nonirradiated yield function.*

One important fact should be noted. In order to achieve complete chemical transformation the initial $C_2F_4Cl_2$ molecule has to be efficiently decomposed by the low energy electrons, while the Cl_2 product should be unaffected. This is achieved by the *selectivity* and particular *energy dependence* of the initial step of the reaction which is DEA.

Previous results with high resolution laser photoelectron attachment spectroscopy have shown that the DEA cross-section to gas phase Cl_2 behaves according to *p-wave* attachment, resulting in a narrow peak at 50 meV with a cross-section of about 2.5×10^{-20} m^2 [79]. On the other hand, the DEA cross-section to $C_2F_4Cl_2$ is about one order of magnitude higher (2×10^{-19} m^2). Moreover the DEA to $C_2F_4Cl_2$ is operative at a much broader energy range, which makes the reaction more effective. Also perfluorinated byproducts are not affected at 1 eV since the DEA processes are energetically not accessible.

Based on these facts we can further assume that the entire film of several

monolayers will be transformed within the irradiated area: while the depth to monitor the Cl_2 concentration via Cl^- desorption is only on the order of 1 monolayer, one can assume that transformation proceeds from the surface layer to the following layers. Since the product Cl_2 (and the perfluorinated by-products) only weakly interact with subexcitation electrons (see above), they can penetrate deeper into the film thereby transforming layer by layer.

6.1.8 ESD from $C_2F_4Cl_2$ in submonolayer amounts

We have investigated the ion desorption following EA to $C_2F_4Cl_2$ molecules adsorbed in submonolayer amounts on top of rare gas solids as a spacer. A relatively thick (> 10 ML) noble gas film is used in order to ensure that the image charge induced in the gold substrate is screened and does not affect desorption. Accordingly, inertness and smaller polarizability of the noble atoms reduces the perturbations to DEA processes and correlations to gas phase results may be done. In general, under such conditions, desorption resonances down to 1 eV may be observed, even if they are suppressed in ESD measurements from pure films (in multilayer films the suppression may originate from higher polarizability of the medium, change in molecule orientation at the surface with film thickness, charge accumulation etc.).

Figures 6.14 and 6.15 show the Cl^- and F^- desorption from $C_2F_4Cl_2$ molecules adsorbed at different concentrations on top of the 15 ML film of Xe, deposited onto the gold substrate cryogenically cooled down to 30 K. The spectra are recorded under 50 nA electron current with an energy resolution of < 0.2 eV in the case of Cl^- but (due to technical reasons) > 0.3 eV in the case of F^-. The submonolayer amounts are obtained by the procedure described in the experimental section at an estimated accuracy of 50%.

From Fig. 6.14 we can clearly distinguish three Cl^- desorption resonances in the energy range $0 - 10$ eV. The first two features peaking at 1 eV and 2.3 eV have also been observed under single collision conditions appearing at 0.3 eV and 2.5 eV, respectively. The shift to higher energy of the first resonance is considered due to the polarization influence of Xe film. The third feature near 8 eV was observed from pure $C_2F_4Cl_2$ film at 8.3 eV and was attributed to originate from core-excited resonances. As seen on Fig. 6.14,

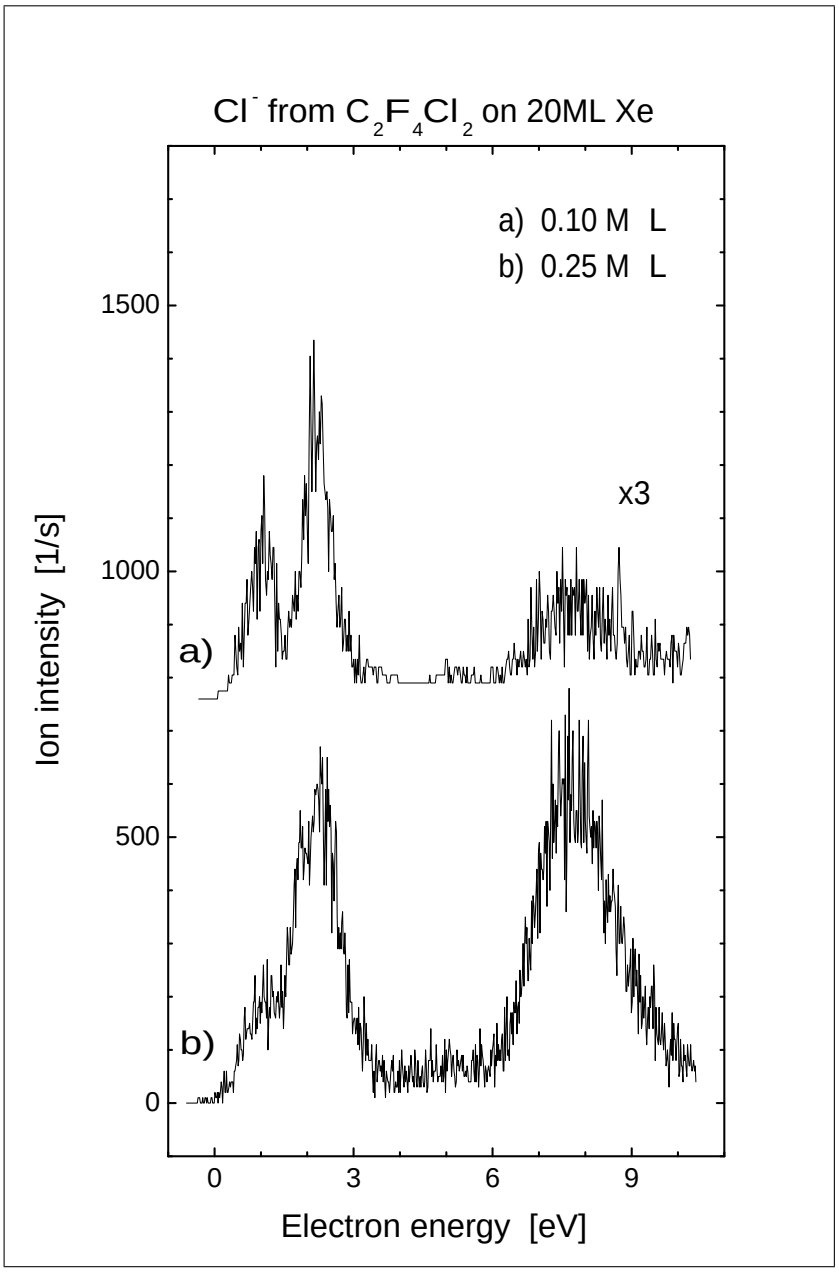

Figure 6.14: *Desorption of Cl^- from $C_2F_4Cl_2$ at the indicated coverage on top of a 15 ML film of Xe.*

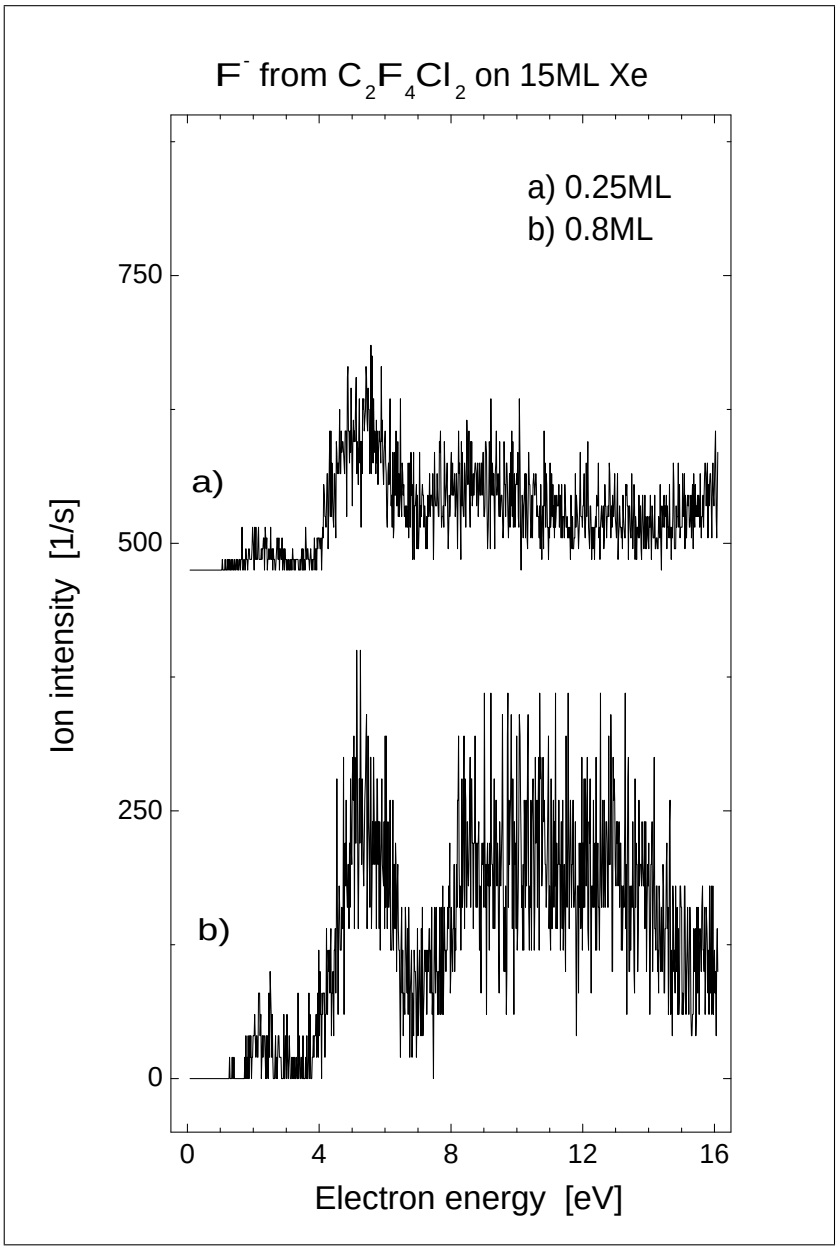

Figure 6.15: *Desorption of F^- from $C_2F_4Cl_2$ at the indicated coverage on top of a 15 ML film of Xe.*

the branching ration between the intensity of 8.3 feature and the lower lying resonances changes with $C_2F_4Cl_2$ concentration at the surface. At coverages of about 0.1 ML the intensity of 8 eV feature is suppressed. Increasing the $C_2F_4Cl_2$ coverage to about 0.25 ML changes the branching ratio in favor of the 8 eV peak. After completion of 1 ML the desorption yield is similar to that obtained from a multilayer film of $C_2F_4Cl_2$ molecules deposited directly onto the gold substrate, Fig. 6.2. The desorption enhancement at 8 eV with $C_2F_4Cl_2$ coverage can be explained by the polarization influence of the environment on intermediate ion formation as discussed extensively in the section *"Medium enhanced DEA"*. The polarization energy V_p of the NIR varies according to the polarizability of the medium in which it is solvated. Because the polarizabilty of $C_2F_4Cl_2$ is higher than that of Xe ($\alpha(C_2F_4Cl_2)$ = 8.5 Å^3, α(Xe) = 4.04 Å^3 [68]), the solvation energy of an intermediate ion decreases when reducing the concentration of $C_2F_4Cl_2$ from 1 ML to 0.1ML. Accordingly, the blue shift in NIR formation may result in conversion of the core excited closed channel resonance (at $>$ 1ML) into core excited open channel resonance (at $<$ 0.1ML). Decay of the $C_2F_4Cl_2^{\#-}$ intermediate ion via autodetachment at reduced concentrations is then more pronounced and a decrease in desorption intensity may be observed.

As Fig. 6.15 shows, the F^- yielding is weaker when compared with that of Cl^-. In order to obtain a reliable signal, higher $C_2F_4Cl_2$ concentrations must be used. The yield function shows three resonances peaking at 2.3 eV, 5.3 eV and 9 eV for the concentrations of about 0.25 ML. Note, the peak positions are estimated with high uncertainty (±0.4 eV) due to insufficient energy resolution of the beam. Suppression of the lowest lying resonance is not clear and may be induced by unfavorable orientation of the molecule on the Xe layer. Fig. 6.15 clearly shows that the F^- intensity near 12 eV increases at higher $C_2F_4Cl_2$ concentrations ($>$ 0.8 ML). As discussed above, the desorption enhancement at 12.5 eV is most likely activated by polarization effect.

Additionally, for submonolayer concentrations deposited on a Xe film, we have investigated the formation of Cl_2, by means of successive scans. The duration of one scan is 75 s with an electron beam intensity 60 nA.

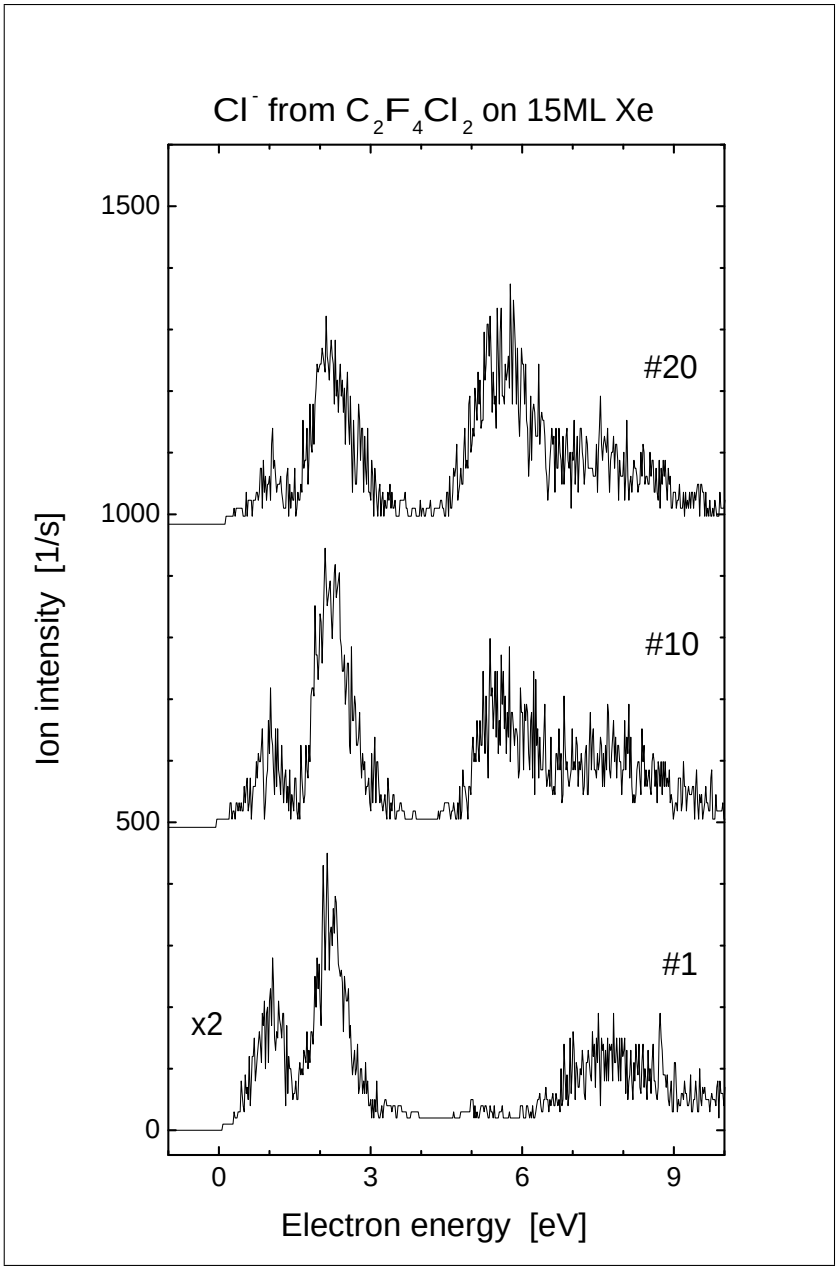

Figure 6.16: *Evolution of Cl^- from a 0.1 ML film of $C_2F_4Cl_2$ deposited on top of 15 ML film of Xe with number of successive scans.*

Fig. 6.16 illustrates the evolution of the Cl^- desorption signal with number of energy scans. As can clearly be seen, even at submonolayer coverages the new feature near 5.8 eV (due to Cl_2) appears and starts to predominate after 20 repetitive scans. Small increase in intensity of 2.2 eV resonance can be observed at the same time. This may also be attributed to Cl_2 formation at the surface, since Cl_2 has a resonant state near 2 eV as was shown by earlier ESD measurements [74]. There are more aspects, which can be considered in order to explain molecular chlorine synthesis even at reduced $C_2F_4Cl_2$ concentrations:

1. $C_2F_4Cl_2$ may form a small clusters at the surface as was already considered before with CHF_2Cl molecules [80]. Island formation is expected after deposition. Since the dipole moment of $C_2F_4Cl_2$ ($\mu = 0.5$ D, average valued at 300 K) is smaller than that of CHF_2Cl ($\mu = 1.45$ D), aggregation of $C_2F_4Cl_2$ molecules is not expected to be rapid, if taking place at all. However, if islands are formed, the above discussed secondary process operative at multilayer amounts may take place.

2. Cl_2 may also be formed by interaction of products from separated molecules. However, the fragments formed upon dissociation must gain sufficient kinetic energy to travel through the distances and activate the reaction. The mobility of physisorbed neutral species at the surface is controlled by diffusion energy E_{dif}, which is in the order of 10% of desorption energy [81]. For the negative ions the value is also expected to be a few percent of the polarization energy. As clearly seen from Fig. 6.14, Cl^- ions are desorbing even at 1 eV, therefore secondary reactions may proceed even without cluster formation.

3. Because within the successive scans the sample is exposed to an electron beam of various energy up to 18 eV, molecular chlorine formation observed on submonolayers (Fig. 6.16) may originate directly from a unimolecular reaction as expressed by reaction (6.13a).

6.1.9 Conclusion of results from $C_2F_4Cl_2$

$C_2F_4Cl_2$ was compared under different degrees of aggregation by means of DEA reactions. Under collision free conditions a variety of fragments were observed, namely $Cl^-, Cl_2^-, F^-, ClF^-, CClF_2^-$ and $C_2F_4Cl^-$. When going to homogeneous clusters, anionic parent has been detected, which indicates that the $C_2F_4Cl_2$ molecule possesses a positive electron affinity. Additionally to fragment ions observed in the gas phase, solvated anions of the form $M_n{\cdot}Cl^-$ for $(n = 1 - 4)$, $M{\cdot}F^-$ and M_n^- for $(n = 1 - 4)$ were detected. In both experiments (gas and cluster), generation of the anions dominates at energies below 4 eV. Ion formation at higher energies is virtually suppressed. Upon condensation of $C_2F_4Cl_2$ at cryogenic temperatures, desorption of negative species is restricted only to three fragments: Cl^-, F^- and Cl_2^-, with desorption yields appearing usually at higher energies > 2 eV. The desorption results may be summarized as follows:

- Cl^-: All resonant states yielding Cl^- in the gas phase could clearly be resolved in condensed phase when $C_2F_4Cl_2$ was deposited in submonolayer amounts on top of the Xe film as a spacer.

- F^-: The ion yield shows all resonances seen in the gas phase. In addition, a desorption resonance near 5 eV was observed.

- Cl_2^-: desorption yield occurs only at 8.3 eV and lower lying resonances observed in the gas phase at 0.7 eV and 2.5 eV are suppressed.

Upon irradiation of condensed $C_2F_4Cl_2$, formation of Cl_2 at the surface was observed. Synthesis of molecular chlorine was demonstrated by energy and temperature dependence of Cl^- desorption. The reaction leading to Cl_2 formation is dependent on the primary electron energy showing a resonant behaviour in the energy range $1 - 18$ eV. The reaction is more pronounced near 10 eV and below 3 eV. The possible reaction routes, which can initiate the synthesis at subexcitation energies are proposed. It is likely that in addition to direct unimolecular reaction, secondary reactions must be considered in order to explain the Cl_2 formation at subexcitation energies. In any case, DEA must be the initial molecular reaction. Upon the extended

irradiation of the pure $C_2F_4Cl_2$ film at 1 eV, chemical transformation of the initial molecule into Cl_2 plus perfluorineted compounds proceeds completely.

Cl_2 formation was observed even after irradiation of $C_2F_4Cl_2$ at reduced concentrations. However, the molecules were irradiated only by means of successive scans and further investigations must be done in order to identify the reaction routes.

We have recorded the vibrational spectra of the irradiated and nonirradiated film of $C_2F_4Cl_2$ using the infrared reflexion-absorption spectroscopy IRAS (Berlin) and electron energy loss spectroscopy EELS (in collaboration with Prof. Petra Swiderek, Koeln) in order to identify formed perfluorocompounds. The observation from these preliminary experiments are not conclusive so far (see Appendix).

6.2 Electron attachment to SF_5CF_3 molecules

Trifluoromethysulphur pentafluoride (SF_5CF_3) as a potent greenhouse molecule has recently been discovered in the stratosphere. The molecule possesses several strong IR bands between $800 - 1300$ cm^{-1} with absorption cross-sections ranging in $10^{-18} - 10^{-17}$ cm^2, resulting in the largest radiative forcing on a per molecule basis of all gases in the atmosphere [17, 82, 83]. The global warming potential (GWP) has been estimated to be around 18500 [84] and is thus the second largest of known greenhouse molecules and comparable with SF_6 (22200). Since the measured atmospheric concentration of SF_5CF_3 is of 0.12 ppt (with the tendency to increase at a rate of about 6 % per year) [17], it still constitutes only a few hundredths of a percent of a total antrophogenic radiative forcing. However, the predicted mesospheric lifetime of the molecule being around 1000 years, gives the potential to influence the climate far into the future.

The sources of the SF_5CF_3 are not yet clearly identified, but trends in concentration of SF_6 and SF_5CF_3 have tracked each other very closely. Therefore, it has been suggested that SF_5CF_3 may be generated from breakdown products of SF_6 [17].

In contrast to SF_6, as a molecule with one of the highest cross-sections for

thermal electron attachment forming *nondissociative* long lived SF_6^-, recent studies on electron attachment to gas phase SF_5CF_3 have shown very effective decomposition into $SF_5^- + CF_3$ at very low energies. Existence of low energy resonances of dissociative character as found in SF_5CF_3 may directly be related to the heterogeneous photochemical activity of the molecule [85, 86]. Photo-induced decomposition of the molecules adsorbed on dust or aerosols (containing weakly bound excess electrons) in the stratosphere could then occur at wavelengths where the gas phase molecules are photochemically inactive, reducing thus their lifetimes in the atmosphere.

In this section we will present results from electron attachment processes on SF_5CF_3 molecules condensed in multilayer amounts directly onto the gold substrate as well as SF_5CF_3 coadsorbed on top of Xe and H_2O films. The aim of the present investigations is to reveal some information about the reactivity of the compound toward low energy electrons when coupled to different environments. Similarly as in $C_2F_4Cl_2$, we will first summarize recent results from the beam experiments, which concern the DEA processes to gas phase SF_5CF_3 and to clusters of SF_5CF_3 [87].

6.2.1 DEA to SF_5CF_3 molecules in the gas phase and clusters

Low energy electron attachment to gas phase SF_5CF_3 under single collision conditions have recently be performed at our laboratory in collaboration with M. Stano (Bratislava) [87]. Only fragment ions have been observed, namely SF_5^-, F^- and CF_3^- with SF_5^- the most dominant channel, Fig. 6.17.

The ratio of the intensities $Z(SF_5^-) : Z(F^-) : Z(CF_3^-)$ is $1000 : 4 : 0.3$, which is slightly different when compared with measurements performed by Sailer *et al.* who obtained a ratio of $1000 : 1 : 4$ [88]. However, both studies show that the heavy SF_5^- is by far the most dominant fragment ion. The difference between the intensities of F^- and CF_3^- is considered due to different collecting conditions in both experiments (i.e. discrimination towards the detection of the fragments with higher kinetic energy in the case of Sailer *et al.*). This, however, demonstrates the limited accuracy in extracting absolute

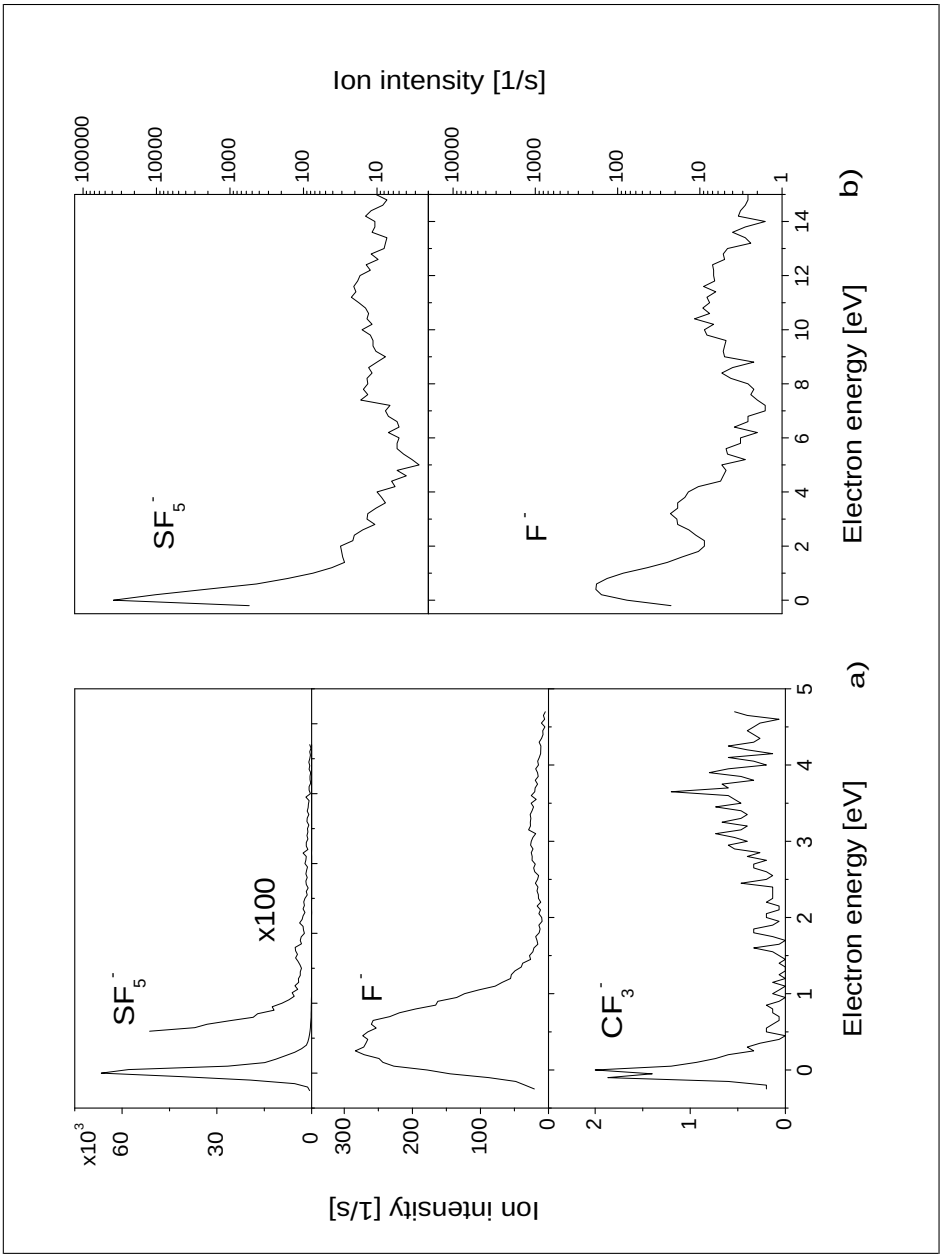

Figure 6.17: ***a)*** *fomration SF_5^-, F^- and CF_3^- via DEA to gas SF_5CF_3* ***b)*** *formation of SF_5^- and F^- in the extended energy range $0-15$ eV.*

cross-sections in beam experiments by comparing the yield intensities.

As mentioned above, the most dominant fragment ion in the gas phase is SF_5^- peaking near 0 eV, suggested to be initiated by a single particle shape resonance,

$$e^- + SF_5CF_3 \rightarrow SF_5CF_3^{\#-} \rightarrow SF_5^- + CF_3 \quad with \quad \Delta H_0 = -0.3\ eV \quad (6.20)$$

the reaction enthalpy was estimated using the bond dissociation energy $D(SF_5 - CF_3) = 3.5$ eV and electron affinity $EA(SF_5) = 3.8$ eV [68, 77, 88]. The reaction (6.20) is thus exothermic by -0.3 eV, which is completely different when compared with electron attachment processes to SF_6. In that case, the reaction generating $SF_5^- + F$ is either endothermic or subjected to an activation barrier, which results in formation of a metastable parent ion SF_6^- near 0 eV. Contrary to it $SF_5CF_3^-$ was not observed under collision free conditions, but it does exist as it is shown by the cluster measurements.

The absolute cross-section of the reaction (6.20) reaches values of 1×10^{-14} cm^2 at energies near 0 eV [82].

F^- may then be formed either by cleavage of the $S - F$ or $C - F$ bond,

$$e^- + SF_5CF_3 \rightarrow SF_5CF_3^{\#-} \rightarrow F^- + SF_4CF_3 \quad with\ \Delta H_0 = 0.5\ eV \quad (6.21a)$$

$$e^- + SF_5CF_3 \rightarrow SF_5CF_3^{\#-} \rightarrow F^- + SF_5CF_2 \quad with\ \Delta H_0 = 2\ eV \quad (6.21b)$$

Since there are no available dissociation energies for the $S - F$ and the $C - F$ bond in the present molecule, the values have been suggested to be similar as in the non-substituted compounds ($D(SF_5 - F) = 3.94$ eV and $D(CF_3 - F) = 5.56$ eV) [68, 77]. Reaction (6.21a) is then endothermic by 0.5 eV, while reaction (6.21b) is endothermic by 2 eV. From these results it can be concluded that the lowest lying F^- resonance near 0.5 eV is exclusively due to reaction (6.21a).

Contrary to results obtained by Sailer *et al.*, our investigation show only spurious CF_3^- signal peaking at 3.5 eV, Fig. 6.17.a). The small contribution near 0 eV, as seen on the figure, is supposed to arise as the result of electron capture to some decomposition product of the target molecule on the hot filament or to some impurity in the restgas. The reaction leading to CF_3^- is

expressed as

$$e^- + SF_5CF_3 \rightarrow SF_5CF_3^{\#-} \rightarrow CF_3^- + SF_5 \;\; with \;\; \Delta H_0 = 1.8 \; eV \quad (6.22)$$

The reaction enthalpy was estimated using the $F_5S - CF_3$ bond dissociation energy and the electron affinity $EA(CF_3) = 1.72$ eV.

It has been suggested that all observed resonances below 5 eV are initiated by single particle shape resonances, formed by capturing of an extra electron to previously unoccupied molecular orbitals (MOs). An earlier study on total electron attachment cross-section (without mass identification), reported three resonant states for SF_5CF_3 molecule, peaking near 0 eV, 3.5 eV and 11 eV. From Fig. 6.17.b) it can be seen that the 11 eV resonance contributes to formation of SF_5^- and F^-. As will be shown below, in the condensed phase the resonant state near 11 eV very effectively activates F^- desorption.

In addition to fragment ions observed in the gas phase, electron attachment to mixed SF_5CF_3/Ar clusters near 0 eV results in formation of $SF_5CF_3^-$ and solvated fragments in the form $Ar_n{\cdot}SF_5^-$ (n = 1, 2) and $Ar_n{\cdot}SF_5CF_3^-$ (n = $1 - 3$). As expected, the SF_5CF_3 possesses a positive electron affinity, which was earlier estimated to be $EA(SF_5CF_3) = 1.24$ eV [89].

Concerning the results in the cluster measurements, it should be noted that low energy electron attachment is enhanced, but part of the attachment events is channeled into associative attachments, seen by formation of parent anion $SF_5CF_3^-$ and complexes of the form $A_n{\cdot}SF_5CF_3^-$ [87].

6.2.2 ESD from SF_5CF_3 nanofilms

Electron stimulated desorption from SF_5CF_3 condensed directly onto gold substrate in multilayer amounts was investigated in the energy range $0 - 18$ eV. The intensity of the incident-electron beam is about 10 nA with an energy resolution 0.2 eV. The duration of one energy scan is 50 s. Since the charging of the molecular film is operative already within the first energy scan, the position of the desorption peaks are estimated within ± 0.5 eV accuracy.

Fig. 6.18 shows the desorption yields of F^- and F_2^- from a 6 ML and a

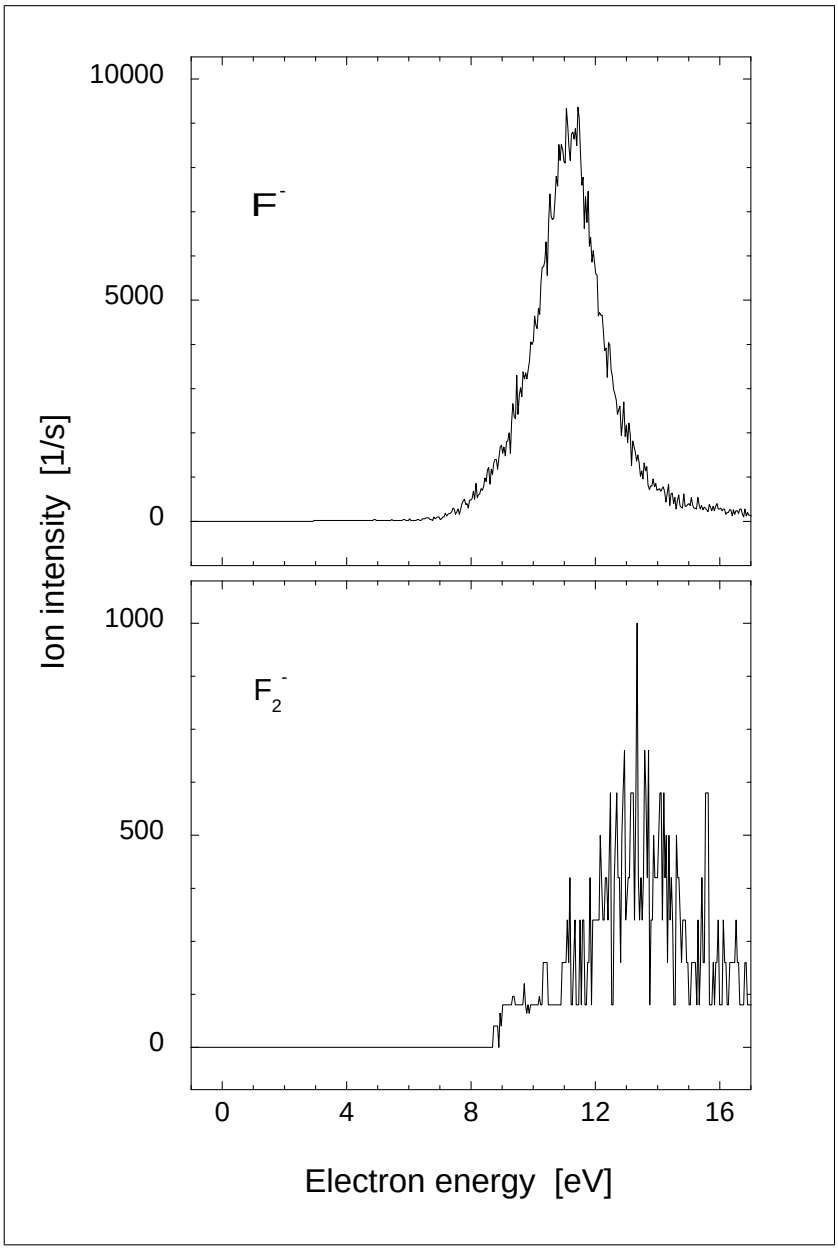

Figure 6.18: *Desorption of F^- and F_2^- from 6 ML and 8 ML film of SF_5CF_3, respectively.*

8 ML film of SF_5CF_3, respectively. The most dominant channel is F^- peaking at 11 eV. It is not clear from observed ion yield, if the F atom originates from $C-F$ or $S-F$ bond cleavage. The F^- formation is most likely initiated by a core excited resonant state, also observed in the gas phase as a broad resonance yielding SF_5^- and F^- with comparable intensities. The suppression of F^- desorption at very low energies mirrors the fact that ions generated via (6.21a) or (6.21b) do not gain enough kinetic energy in order to be ejected into vacuum. The desorption cross-section of F^- at 11 eV is estimated to be $\sigma_{\mathrm{des}}(F^-) \approx 10^{-16}$ cm^2, when compared with the desorption cross-section of $Cl^-/C_2F_4Cl_2$ at 8.3 eV ($\sigma_{\mathrm{des}} = 3 \times 10^{-17}$cm^2). This is by about 2 orders of magnitude higher than its corresponding DEA value in the gas phase at the same energy. The F^- channel at 11 eV is thus strongly enhanced when changing from gas to the condensed phase. This is attributed to the longer lifetime of the NIR when coupled to an environment. This happens in consequence of conversion from an open channel core excited resonance to a closed channel core excited (Feshbach) resonance, see section "*Medium enhanced ESD*". In addition, strong F^- desorption suggest that the involved core excited resonance possesses appreciable $S-F$ or $C-F$ antibonding character, *i.e.*, two electrons are in antibonding molecular orbital (σ^* MO).

The second desorption product F_2^- appears near 14 eV and may be generated by cleavage of $C-F$ and/or $S-F$ bonds within the same molecule. Since F_2^- was not observed neither from gas phase molecules nor from the homogeneous clusters, it is expected that post dissociation interaction of generated F^- ions with surrounding molecules are involved in the observed F_2^- desorption yield,

$$F^- + SF_5CF_3 \rightarrow F_2^- + SF_5CF_2 \tag{6.23}$$

$$F^- + SF_5CF_3 \rightarrow F_2^- + SF_4CF_3 \tag{6.24}$$

Desorption of SF_5^- and CF_3^- (observed in the gas phase and clusters) is totally suppressed as it is generally expected. In the case of polyatomic molecules the energy dissipation in the decomposition of the precursor ion $SF_5CF_3^{\#-}$ may take place and the desorption of the polyatomic species be-

comes very unlikely.

As extensively discussed above, suppression of desorption below 10 eV does not automatically imply the suppression of the dissociation channel at the surface. The charging behaviour of the film indicates that the electron attachment processes are readily operative at these energies. To which degree the charge accumulation contributes to associative or dissociative processes remains under question. However, when proceeding from single collision conditions to clusters, increase in associative attachment has been observed [87].

6.2.3 ESD from SF_5CF_3 deposited onto Xe and H_2O films

We have further studied the behaviour of the ion desorption from SF_5CF_3 deposited in submonolayer amounts on top of the Xe film and amorphous water ice independently. The recorded spectra are obtained under 10 nA incident-electron beam intensity with an energy resolution of about 0.2 eV. The molecular films are prepared at a substrate temperature of about 30 K.

Desorption from SF_5CF_3 at reduced concentrations on top of multilayer Xe film and water ice is restricted only to one fragment, namely F^-. The F_2^- desorption was not observed, which point towards its generation via PDIs when used SF_5CF_3 in multilayer amounts.

Fig. 6.19 illustrates the evolution of F^- with SF_5CF_3 concentration deposited onto Xe film as a spacer. The yield intensity increases linearly with coverage and after the completion of one monolayer the increase is gradually weaker. The desorption intensity tends to saturate at coverages of about 8 MLs (not shown here). Additionally, for coverages of about 0.25 ML, a new resonance peaking at 4 eV can be observed. This feature may be viewed as the high energy tale of the F^- DEA resonance seen in the gas phase at 3.5 eV.

Electron stimulated desorption from molecules embedded in an environment of polar molecules has attracted considerable attention since the report of giant enhancements in Cl^- and F^- desorption from CF_2Cl_2 deposited on

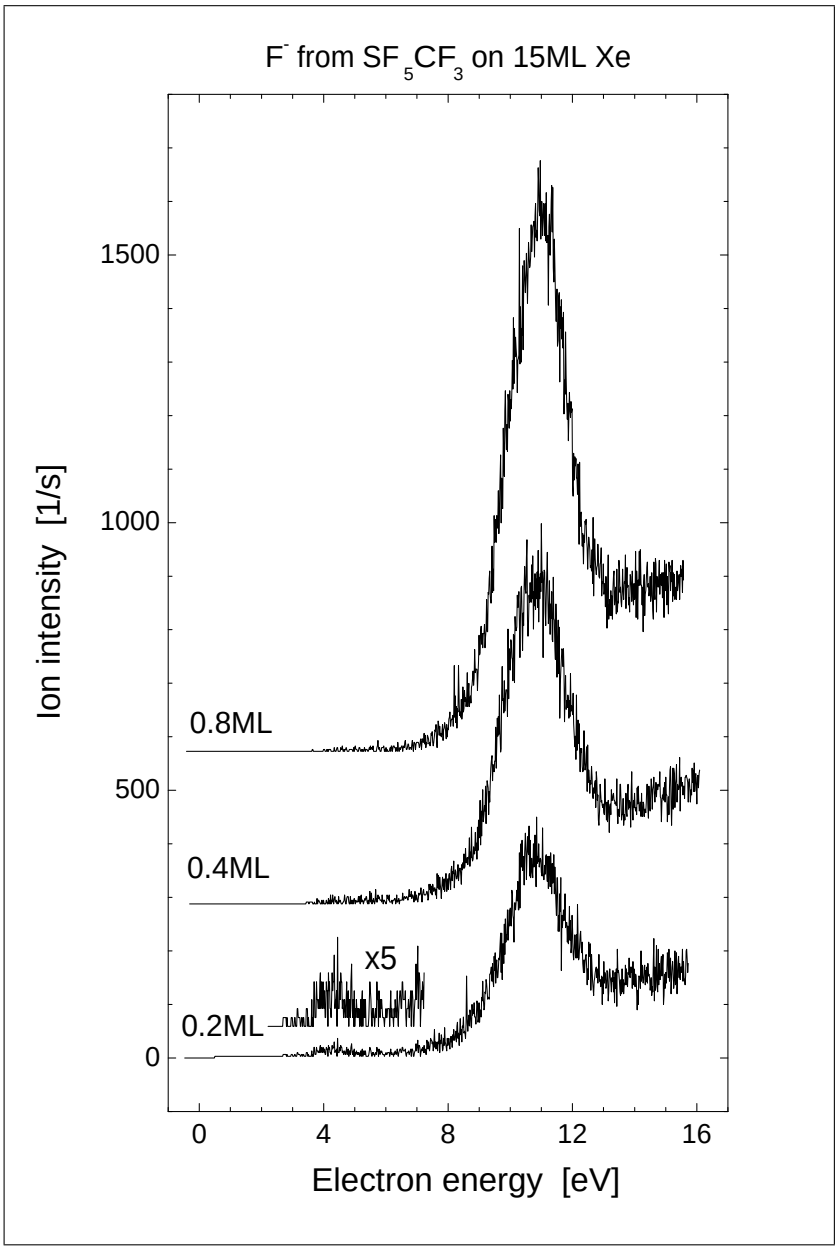

Figure 6.19: *Evolution of F^- with SF_5CF_3 concentration on top of* 15 *ML film of Xe*

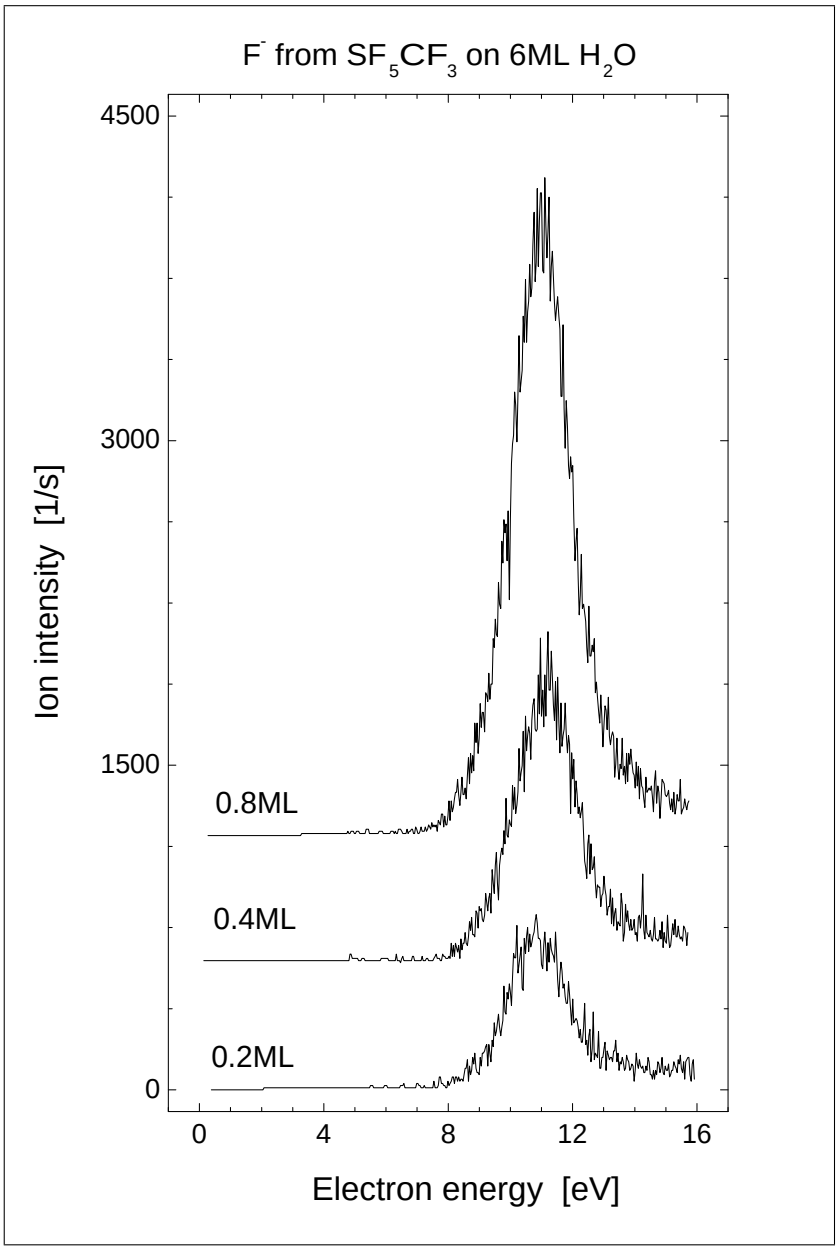

Figure 6.20: *Evolution of F^- with SF_5CF_3 concentration on top of 6 ML amorphous ice.*

top of the ammonia or water ice through 250 eV incident electrons [18, 55]. These enhancements were attributed to dissociation of CF_2Cl_2 by capture of electrons solvated in polar environment. Recent ESD experiments using low energy electrons, did not show any enhancements in ion desorption from CF_2Cl_2 deposited on top of polar molecules [90]. On the other hand, charge trapping experiments have demonstrated that EA processes are enhanced under these conditions [91]. Preliminary experiments on $C_2F_4Cl_2$ adsorbed in submonolayer amounts on NH_3 in fact indicate ESD enhancement at very low energy, see Appendix.

Fig. 6.20 illustrates the evolution of F^- with SF_5CF_3 concentration on top of amorphous water ice. The ion yields are similar to that obtained when SF_5CF_3 is coadsorbed on Xe. However, by comparing the absolute intensities, it can be seen that desorption from water ice is more efficient than from Xe. Although the accuracy in reproducing count rates is not better than the difference in the intensities between Xe and H_2O, the repeated measurements point toward the higher intensity from the water layer. This is a surprising result, as the desorption of O^- from O_2 is suppressed when coadsorbed on water ice [92, 93]. The desorption quenching was explained by penetration of deposited O_2 molecules into the pores, which are present in the case of amorphous ices. From observed desorption intensity, penetration into pores may thus not occur for SF_5CF_3.

One can then speculate why the desorption intensity from water ice exceeds that from Xe. The main question is, if within the lifetime of the NIR the water dipoles are able to respond to the negative charge and provide a polarization trap. However, high desorption intensity suggest that the F^- ions are generated with appreciable kinetic energy. Moreover, the favorable orientation of the anionic precursor at water surface may enhance the desorption.

A further aspect concerns substrate induced reactions. Water possesses a series of resonances in th energy range $6 - 12$ eV yielding H^- [93]. The charge and energy transfer from these resonant states may then enhance the desorption yield of the SF_5CF_3 molecule. Such reactions have been observed for molecules deposited in submonolayer amounts on noble gas film,

by forming the electron-exciton complexes of the rare gas atom. The energy and charge from these complexes is then efficiently transfered into adsorbed molecule, seen by sharp enhancements in desorption yield [53]. However, for the present system we could not observe mentioned enhancements.

6.2.4 Conclusion of results from SF_5CF_3

DEA to gas SF_5CF_3 lead to the formation of SF_5^-, F^- and CF_3^-. SF_5^- is the most dominant channel appearing near 0 eV. Cluster measurements revealed the formation of the parent anion $SF_5CF_3^-$ and solvated fragments in the form $Ar_n{\cdot}SF_5^-(n = 1, 2)$ and $Ar_n{\cdot}SF_5CF_3^-(n = 1 - 3)$. The observation of the parent anion indicates that the molecule possesses a positive electron affinity.

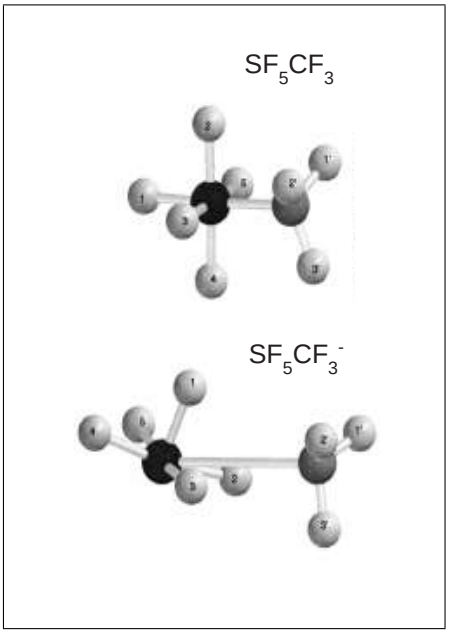

Figure 6.21: *Structures of SF_5CF_3 and $SF_5CF_3^-$ according to Miller et al. [89]*

Condensed phase measurements show desorption of F^- and F_2^- appearing at 11 eV and 14 eV, respectively. The fragment ion F_2^- was observed only in the condensed phase and is expected to be formed via PDIs of the F^- ions. Desorption of F^- from pure film of SF_5CF_3 shows an intense resonance peak. As frequently observed before, the lower lying resonances seen in DEA to gas SF_5CF_3 have completely been suppressed in desorption. However, the film charging indicates that attachment processes are effective in the low energy domain. To what degree the observed charging is controlled by dissociative or associative processes remains under question, but enhancement in associative processes when going from gas phase to clusters has been observed.

As seen from Fig. 6.21 the structure of the SF_5CF_3 changes consider-

ably upon forming the negative ion $SF_5CF_3^-$. The calculations show that the trapped electron is located on the SF_5 site causing its rotation with prolonging the $S-C$ bond almost twice at the same time [89]. The cleavage of the weaker $S-C$ bond then results in formation of $SF_5^- + CF_3$ at thermal electron energies in the gas phase. As suggested by Miller *et al.*, the weak $S-C$ bond indicates that the $SF_5CF_3^-$ may only exist in an environments at low temperatures.

When SF_5CF_3 is adsorbed on top of the multilayer Xe film, new feature near 4 eV in desorption of F^- may be distinguished. This resonance was assigned to the resonant state seen in the gas phase at 3.5 eV yielding SF_5^- and F^-. F^- desorption yield from SF_5CF_3 adsorbed on top of the amorphous ice indicates some enhancement in intensity when compared with that obtained from Xe. However, the origin of the observed enhancement is not easy to identify, since all influences like polarization effect, orientation of the molecule at the surface and substrate mediated reactions may partially contribute to the final increase in F^- desorption intensity.

Regarding the problem of SF_5CF_3 adsorption on dust or ice particles in the Earth's stratosphere, the UV radiation may liberate the electrons which can then induce DEA reactions at low energies. From our ESD spectra, however, we can only conclude that the dissociative state of $SF_5CF_3^-$ near 11 eV cannot be accessed by photoelectrons beyond the Ly_α line and therefore may not play a significant role in the chemistry of the atmosphere.